

Final Report

Intelligent Controls for Net-Zero Energy Buildings

Submitted

to

Paul Giles, Project officer

U.S. Department of Energy

National Energy Technology Laboratory

By

Haorong Li, Ph.D., Associate Professor

Yong Cho, Ph.D., Associate Professor

Dongming Peng, Ph.D. Associate Professor

University of Nebraska-Lincoln

1/28/2012

Contents

| | |
|--|----|
| 1. Introduction and Background..... | 4 |
| 2. Development of Low-cost Building Information Modeling Methods..... | 6 |
| 2.1 Floor Plan Frame Extraction..... | 6 |
| 2.1.1 Feature Extraction..... | 6 |
| 2.1.2 Feature Classification..... | 7 |
| 2.2 Vertical View Information Extraction..... | 8 |
| 2.2.1 Window Detection..... | 8 |
| 2.2.2 House Surface Layout Detection..... | 11 |
| 2.3 Methods for As-Built Building Information Collection and Modeling..... | 13 |
| 3. Development of Building Performance Auditing and Optimal Retrofit Analysis Tools..... | 14 |
| 3.1 Development of 3D Building Performance Model using BIM and Thermographic Technology..... | 14 |
| 3.1.1 Methodology..... | 14 |
| 3.1.2 Field Test..... | 18 |
| 3.2 Development of Building Envelope Recognition Algorithm..... | 21 |
| 3.2.1 Methodology..... | 21 |
| 3.2.2 EXPERIMENTAL RESULTS..... | 25 |
| 3.3 Development of Web-Based 3d Building Performance Model..... | 27 |
| 3.3.1 Methodology..... | 27 |
| 3.3.2 Creating Data..... | 27 |
| 3.3.3 Converting 3D Point Cloud Data to Geographic Coordinate Data..... | 28 |
| 3.3.4 Converting BIM model to KMZ, KML 3D Model..... | 29 |
| 3.3.5 BIM with 3D Geographic Data in Google Earth Pro™..... | 30 |
| 3.3.6 Thermal Information Marked by Different Colors..... | 32 |
| 3.4 Hardware Development of a New 3D LiDAR System..... | 32 |

| | |
|---|----|
| 4. Development of Automated Performance Diagnostics and Optimal Controls..... | 33 |
| 4.1 Building field data collection and analysis | 33 |
| 4.2 Building American (BA) Benchmark | 34 |
| 4.3 Standard Building Performance based on the BA Benchmark..... | 34 |
| 4.4 Building Thermal Performance Diagnosis Methods | 34 |
| 4.5 Building Thermal Performance Diagnosis based on the Benchmark..... | 37 |
| 4.6 Thermal mass effects..... | 38 |
| 4.7 Infiltration effects..... | 41 |
| 4.8 Blower Test for the whole building leakage | 41 |
| 4.8.1 Preparing for a Blower Door Test | 42 |
| 4.8.2 Blower Door Installation | 43 |
| 4.8.3 Test Procedure | 43 |
| 4.8.4 Flow Rate Reading..... | 44 |
| 4.8.5 Blower Door Test Result | 45 |
| 5. CONCLUSION | 48 |
| REFERENCES | 50 |

1. Introduction and Background

Buildings account for about 40% of the primary energy usage, 71% of the electricity in the U.S.(U.S. DOE 2008; EIA 2009), and, yet, they receive much less public attention than fuel economy or new technologies for automobiles or alternative sources or distribution systems for power generation. The US DOE Build America Program (NREL 2008) set a goal of reducing the average energy use of housing by 40% to 70%. Especially, the existing residential buildings comprise the single largest contributor to U.S. energy consumption and greenhouse gas emissions (>50%) which is applied to over more than 120 million buildings (>95% of the total number of buildings). Exacerbating these problems is the fact that the average age of such buildings is over 50 years, with about 85% of buildings built before 2000(U.S. DOE 2008). However, millions of decision makers of these buildings usually lack sufficient information or tools for measuring their building's energy performance and they are faced with a dizzying array of expensive products and services for energy efficiency retrofit with long, uncertain payback periods. Consequently, existing buildings represent the greatest opportunity to improve building energy efficiency and reduce environmental impacts. Most of the current research is related to high performance technologies for new construction and large commercial buildings. In contrast, the primary focus for this study would be on existing small commercial and residential buildings where decision support tools are lacking.

The disconnect between existing high performance building products and the willingness of decision makers to choose those products is likely due to the complexity of building systems and the marketplace and the lack of adequate feedback loops between decision makers and outcomes associated with the different stages of the building lifecycle. In particular, there is still a lack of: 1) rapid and low-cost as-built data collection techniques for Building Information Modeling of existing buildings(Schlueter 2008); 2) metrics and measurements for evaluating overall building performance (including energy and occupant issues); 3) adequate measurements and integrated intelligence for evaluating component performance; 4) tools and information geared to non-expert decision makers (e.g., owners, occupants); and 5) evidence that buildings touted as high performance actually perform well.

Previous work has focused on some aspects of the problems above. However, several gaps remain that will be addressed in this project including:

- Lack of perception-based rapid & low-cost data collection tools for as-built BIM design and thermal performance of existing buildings
- Lack of integrated tools and data for analyzing the performance and opportunities for improvement in existing buildings, and

- Lack of connectivity between building performance information and decision makers

The goal of this project is to develop and demonstrate enabling technologies that can empower homeowners to convert their homes into net-zero energy buildings in a cost-effective manner. The project objectives and expected outcomes are as follows:

- To develop rapid and scalable building information collection and modeling technologies that can obtain and process “as-built” building information in an automated or semi-automated manner.
- To identify low-cost measurements and develop low-cost virtual sensors that can monitor building operations in a plug-n-play and low-cost manner.
- To integrate and demonstrate low-cost building information modeling (BIM) technologies.
- To develop decision support tools which can empower building owners to perform energy auditing and retrofit analysis.
- To develop and demonstrate low-cost automated diagnostics and optimal control technologies which can improve building energy efficiency in a continual manner.

2. Development of Low-cost Building Information Modeling Methods

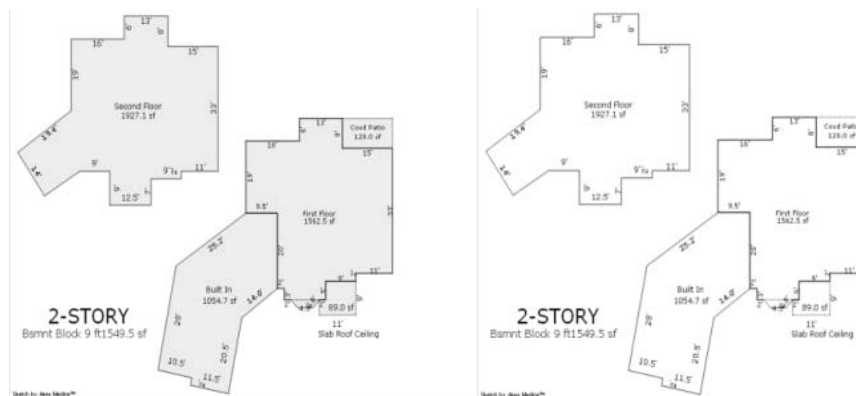
2.1 Floor Plan Frame Extraction

A floor plan, from which geometry information can be obtained, is an important document for buildings and houses. All the floor plan images tested in this research can be easily accessed from public online databases where the floor plan images are made by being scanned from hard copies into JPG or PDF files. Sections 2.1.1 and 2.1.2 describe how the floor plan images are processed to extract useful geometric information.

2.1.1 Feature Extraction

For some scanned floor plan images, the floor area has a background color. It is necessary to delete the background color before processing the floor plan image.

As a first step, the occurrences of each pixel value are recorded. If the count of the second most occurred pixel value exceeds 50000, this pixel value is assumed as the value of the background color. Those pixels with a background color pixel value are changed to the value of the most occurred pixel value to eliminate the background color. As shown in Figure1 (b), the background color is eliminated in the revised image.



(a)(b)

Figure1 (a) Original image; (b) Revised image

Most of the floor plans generally contain texts and symbols in the images. Such noisy information also affects our floor plan recognition. In the developed algorithm, a small isolated pixel group will be eliminated if the amount of pixels in the group is less than 100. As shown in Figure2 (b), all the texts and symbols are deleted.

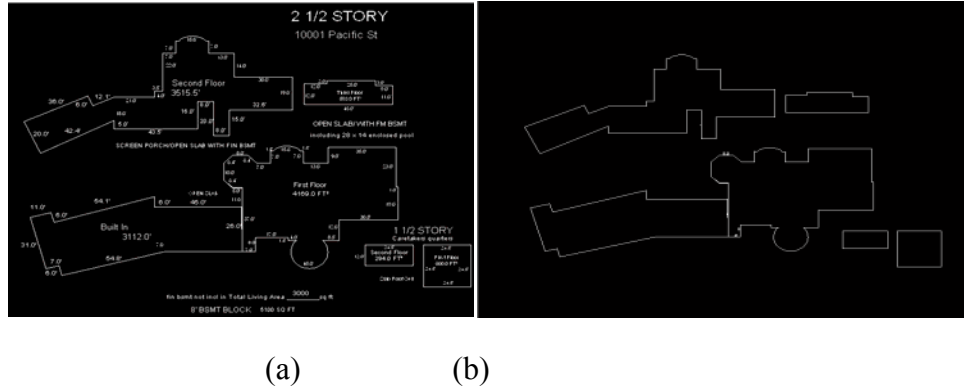


Figure2 (a) Original Image; (b) Revised image

2.1.2 Feature Classification

With the new floor plan after feature extraction, floor plan's feature classification, recognition and vectorization will be realized. The understanding of floor plans is composed with mainly three kinds of pattern recognition including straight line recognition, slashed line recognition and curved recognition. All lines' necessary information is extracted after these pattern recognitions are processed. Then the recognized line information will be used for a 3D modeling process later. Rate of change (slope) is the major criteria for differentiating these lines.

a) Straight Line Segmentation

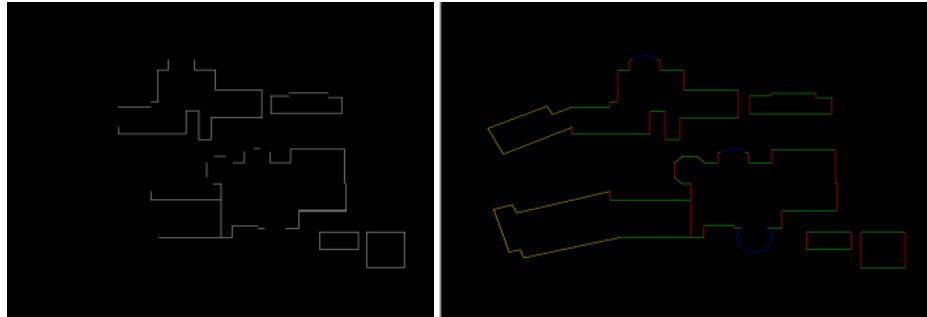
Based on the knowledge that each pixel of a horizontal line exists on the same row, the image can be scanned horizontally, and only those line segments with no less than 4 pixels are kept. After all rows are scanned, the position of each line's end points is recorded. The vertical lines are recognized in the same method replacing rows with columns. In Figure3 (a), all the horizontal and vertical lines are recognized.

b) Slashed and Curved Line Segmentation

This phase is aimed at recognizing slashed lines and curves that contribute to the closure of floor plan frames. First, all the recognized horizontal and vertical lines are deleted from floor plan frames. The pixels left in the image are selected as slashed lines or curved lines if the end points of these line segments match with endpoints of horizontal and vertical line segments. The openings can be located by determining whether they have overlapping ending points or not. No overlap defines the openings.

All the edge points are linked together into lists of coordinate pairs, and the change of slopes on each pixel group is calculated. If the rate of slope change is very fast, and the difference between two adjacent slopes is relatively small, it will be recognized as a curved line segment; otherwise it

is a slashed line segments. Finally, all coordinate pairs are checked to close up any tiny openings if they exist. As shown in Figure 3 (b), slashed lines and curved lines are correctly recognized and are rendered by different colors.



(a) (b)

Figure 3 (a) All recognized horizontal and vertical line segments; (b) Different kinds of the line segments marked by color

2.2 Vertical View Information Extraction

2.2.1 Window Detection

Window detection is an essential process for building thermal modeling in order to do the energy analysis. The position and size of the windows can be calculated with recognition of windows. Recognizing the windows from the RGB images is an issue to be solved.

To solve this problem, Hue, Saturation, and Value (HSV) color space was utilized in our algorithm. In HSV color space, different materials of different brightness in the image have different color, and this characteristic can be used to distinguish windows (Riazet at, 2008). According to brightness in HSV images, main wall area tends to be blue, while windows and other areas tend to be red/green, as shown in Figure 4 (b). Because of the reflection of the glass and other smooth interface, the saturation of windows is always very low. Therefore, for windows, HSV will have (high, low, low) value, and the color tends to be red. The main wall is brighter, so it has larger value in HSV (low, low, high) and tends to be blue. Under some circumstances, the color of the wall is green if it is not bright enough.



(a) (b)

Figure 4 (a) RGB image; (b) HSV image

In the developed algorithm, the RGB images needed to be transformed to HSV color space first. Then based on empirical values of HSV for windows obtained through our tests, it is recognized as a window if the following is satisfied,

$$H > 0.2, S < 0.4, V < 0.4$$

After filtering through HSV segmentation, some parts of image might be recognized as windows by mistake. To assist with HSV segmentation, RGB color segmentation was also added into the developed algorithm. The output of RGB color segmentation is a black and white image, as shown in Figure 5 (b), in which real windows are always a purely white area, while fake windows tend to have many noise points inside because of the different color segmentation characters in different materials (wall surface and glass). As shown in Figure 5 (a), eighteen areas are detected as windows. By utilizing RGB color segmentation, the wrongly detected windows can be successfully deleted if there is any dark point in the window panel area. It can be seen in Figure 5 (c) that twelve wrongly detected windows among eighteen detected windows are deleted, and the rest are recognized as the real windows.



(a)

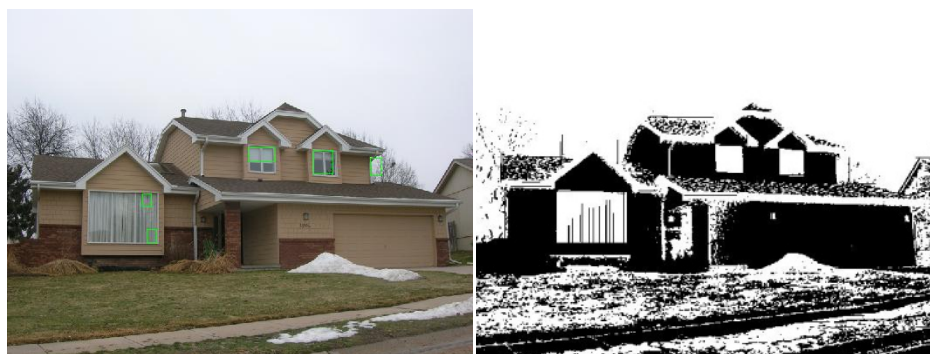
(b)

(c)

Figure 5 (a) Windows detection without RGB color segmentation; (b) RGB color segmentation; (c) windows detection with RGB color segmentation

It is inevitable that some objects in the image can have a bad impact on the window recognition. The most common problem is that the window area is separated by something in front of it or behind it. Vertical or horizontal blinds in big windows can split the window into small strips and cannot be detected correctly through the developed algorithm. After doing image segmentation, the blinds leaf is shown as lines in the white area. To find out whether the lines are strips caused by blinds or are actual window borders, the neighborhood around the lines is checked. If the line is among the white area, it is blinds. Otherwise it is the boundary of the window. In Figure6 (a), the left window is wrongly recognized because there are blinds behind the window. Several lines are created after color segmentation which results in an erroneous window detection as shown in Figure 6 (c). After using the developed algorithm described above, the lines in the window area are eliminated. Then the window can be correctly recognized. As shown in Figure6 (d), six windows are correctly recognized.

According to the boundaries of the windows detected by the algorithm, the bounding boxes are added into the RGB image to be defined as window areas. In this research, about 90 images of different houses were tested; Figure7 shows four examples of windows detection, in which there are several different shapes of windows, such as rectangular, fan-shape, and elliptical. As shown in Figure 7, most of the windows are successfully recognized from the images.



(a)

(b)



(c)

(d)

Figure 6 (a) Wrong window detection; (b) color segmentation; (c) improved color segmentation; (d) improved results with correct window detection



Figure 7 Different shapes of windows being recognized

2.2.2 House Surface Layout Detection

In this section, the objective is to extract the vertical view information from the elevation-view images.

In Section 2.1.2, our edge detection algorithm is utilized to get the edge map of the image as well as delete the lines outside of the border of the house, as shown in Figure8 (b). Secondly, all closed areas are allocated with a different color, and all open lines merged in the same color are highlighted, as shown in Figure8 (c) and (d).

The highlighted lines are then extended in different ways. If the highlighted line is a horizontal or vertical line, it will be extended if the filter threshold can be satisfied. If it is a sliding highlighted line, the line will merge to the closest un-highlighted line. Due to the extension of the highlighted lines, more closed areas will be created. Then the algorithm loops back to the beginning to look for open lines and extend them.

Lastly, black gaps, useless lines, and color bands are removed to obtain a better result. Integrating the window information obtained from Section 3.1, the preliminary vertical house layout is obtained, as shown in Figure 8 (h).

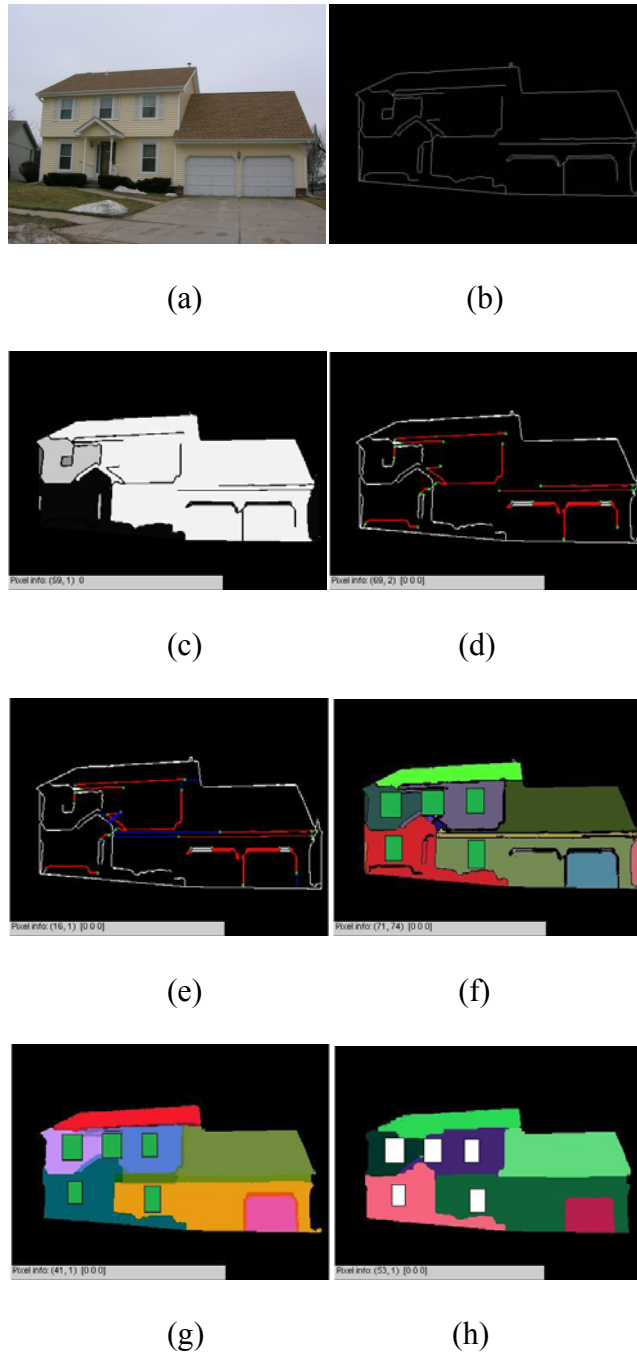


Figure 8 (a) Original image; (b) edge map; (c) merged image colored in gray; (d) highlight lines and end points; (e) lines extension; (f) color result; (g) color result after cleaning black gap and useless lines; (h) color result after removing color band

2.3 Methods for As-Built Building Information Collection and Modeling

Figure 9 is a flow chart to show how the as-built building information can be collected and modeled through our proposed method. As shown in Figure 9, floor plan image and elevation-view images can be downloaded from public online database. The floor plan frame is extracted from the original floor plan image after being processed by the algorithm proposed in section 2.1. Multiple elevation-view images are needed in this research, for example, as shown in Figure 10, two images are front view and east side view of the house. For each side view of the image, it is processed by the algorithm proposed in section 2.2. All the information of house surface layout and openings is obtained after processing multiple images. To build a 3D geometry model through images, image registration algorithm should be utilized. As a similar technique, Mani Golparvar-Fard (Golparvar-Fard 2009) has proposed a method showing the feasibility to create a 3D as-built model with multiple images.

Then the floor plan frame is scaled to fit with the 3D model. In addition, different zones can be created with help of the floor plan frame. The final objective is to make the 3D geometry model ready to be imported into the simulation software for energy analysis.

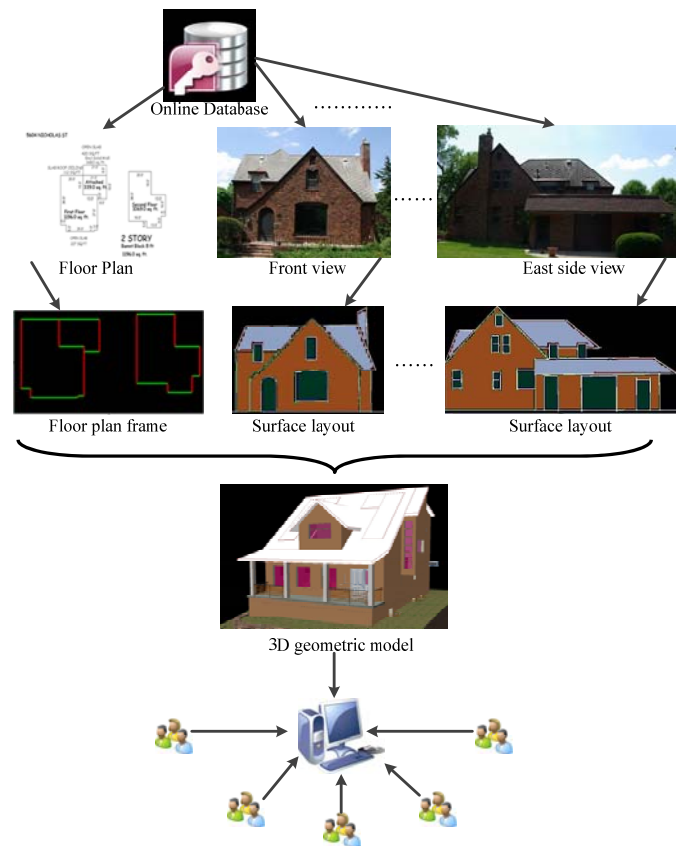


Figure 9 Methods for as-built building information collection and modeling for energy analysis users

3. Development of Building Performance Auditing and Optimal Retrofit Analysis Tools

3.1 Development of 3D Building Performance Model using BIM and Thermographic Technology

3.1.1 Methodology

In this chapter, a method to create a 3D energy performance model is presented. As shown in Figure 10, in the phase of pre-processing, IR camera calibration should be conducted first. Then 3D point clouds and temperature data are obtained from the integrated 3D LIDAR and IR camera system, respectively. Finally, temperature information is mapped to 3D point cloud data to form a 3D energy performance model. The following sections will further discuss system hardware, the functions of IR camera calibration, and data fusion.

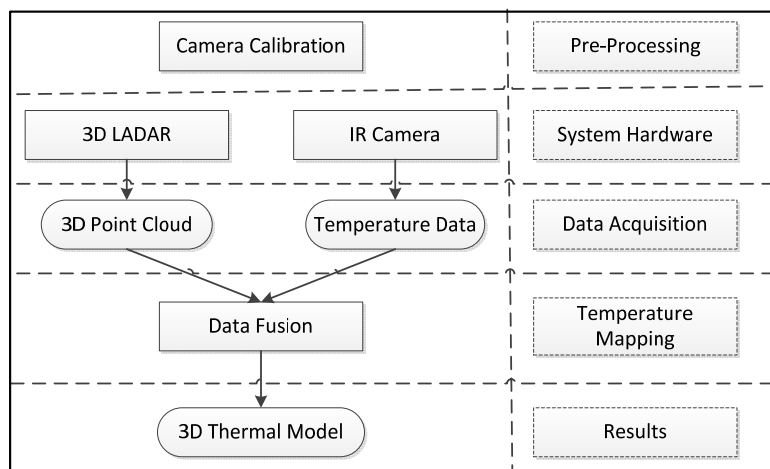


Figure 10. Workflow of creating 3D energy performance model

3.1.1.1 IR Camera Calibration

Camera calibration is an essential process in computer vision and 3D measurement applications because it corrects the image distortion. Among the image distortion, radial and tangential distortions are the worst parts (Ma et al. 2003). To reduce the distortions, the IR camera should be calibrated in advance to obtain intrinsic parameters which include focal length, principal point, skew coefficient, and distortion coefficients (Heikkila and Silven 1997; Bouguet 2010). There are several camera calibration methods introduced elsewhere (Ma et al. 2003; Heikkila and Silven 1997; Bouguet 2010). In our test, Bouguet (2010)'s camera calibration method was adopted. A checkerboard (black and white) was used as an object for testing the function. During the calibration process, the edge detection algorithms were applied to identify the structure of the checkerboard based on the different color, and then the camera parameters could be accurately

calculated (Drennan 2010). Unlike a normal digital camera, however, different colors on the same material cannot be recognized by an IR camera, thus the color of the IR image is rendered based on the temperature difference.

To deal with this issue, we cut out the black parts of the checkerboard, and the new checkerboard was placed in front of a human subject to make the structure of the new checkerboard recognizable in the IR images by using body temperature as a background. Figure 11 shows the eight images that were taken as targets to be tested. In the IR images, the bright parts of the checkerboard were obtained due to the heat from the human body passing through the empty areas. The areas where the heat was blocked by the checkerboard were rendered to dark color in the IR images. Then these eight different IR images were tested in the camera calibration program. In Figure 11, all the IR images were shown in thumbnail format, and the corner extraction process of the first image was also demonstrated. Then the values of the intrinsic parameters were obtained and presented in Table 1.

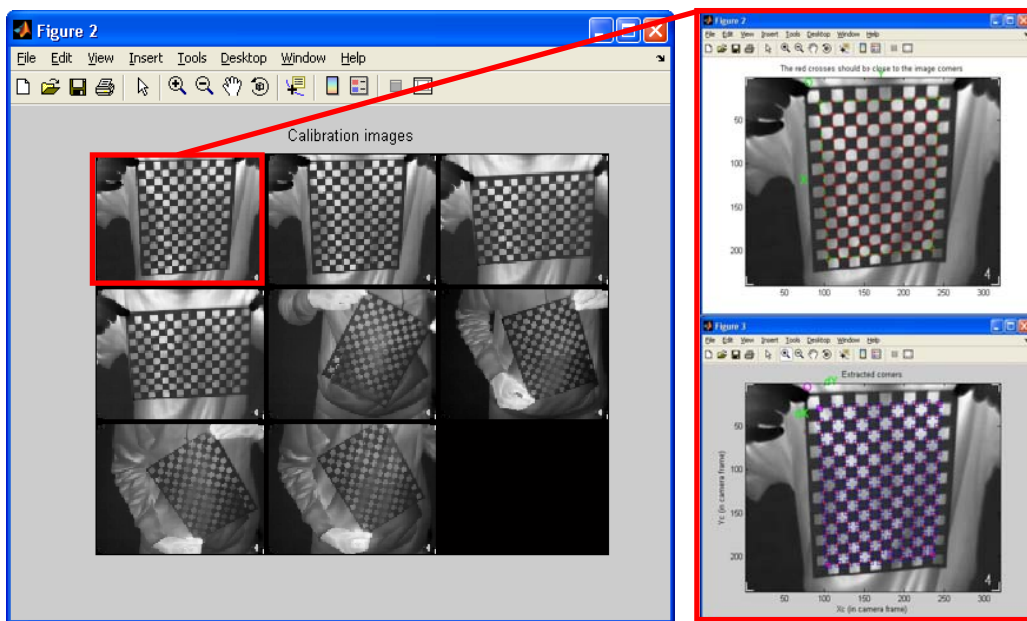


Figure 11. IR Camera Calibration

Table1. Values of the intrinsic parameters

| Intrinsic Parameters | Value |
|-------------------------|---|
| Focal length | [766.21061 724.71580] |
| Principal point | [196.12649 259.10822] |
| Skew coefficient | [0.00000] [0.00000] |
| Distortion coefficients | [-0.26691 0.01693 -0.01586 0.00368 0.00000] |

3.1.1.2 System Hardware and Data Acquisition

This research developed a system integrated by a set of developed LIDAR system (Cho and Diego 2009) and an IR camera, as shown in Figure 12. The developed LIDAR system consists of a 2D laser rangefinder and a pan and tilt unit (PTU). The 2D line scanner can measure the distance between an object and itself through emitting and receiving the laser lights. After it was mounted on the PTU, the LIDAR system was able to 3D scan. As the result of the 3D scanning process, a set of points in a 3D coordinate system is created. These points are defined by X, Y, and Z coordinates which are representative of the external surface of an object. The developed LIDAR system can provide up to 200K points per second from a scene with 8mm accuracy at a 15m distance (Cho and Diego 2009). The IR camera was mounted on top of the laser rangefinder and connected to a PC via an Ethernet interface. One snapshot of the IR camera produces a matrix (320*240) where each element contains a temperature value of the corresponding pixel of the IR image which was created and sent to the PC.



Figure 12. Developed Hybrid 3D LIDAR System

3.1.2.3 Data Fusion

The data fusion process is similar to texture mapping which is a method for adding images as texture to the surfaces of the 3D models. The main difference in the data fusion process is that the temperature data instead of RGB color data will be mapped to a 3D object. In order to map the temperature data to the point cloud correctly, the relationship between 2D temperature data and 3D point cloud has to be built. First, the concept of perspective projection is introduced into our test, and a reference test was made to create a reference plane for the 3D projection. During the reference test, a 120cm*90cm rectangular object was used as a target, and both the laser rangefinder and the IR camera were parallel to the object. The distance between object and system was adjusted to make sure that the object completely filled the IR camera's view. As shown in Figure 13(a), the distance between object and camera is f_{ref} , θ is the IR camera view

angle, and (X_i, Y_i, Z_i) is the coordination of the point cloud in the system coordinate system. Through the calculation several variables could be obtained as follows:

$$f_{ref} = 166\text{cm}, \theta = 39.7^\circ, \text{PixelUnit} = \frac{120}{320} = \frac{90}{240} = 0.375$$

Having the reference plane, all the object parallel to the system can be mapped with temperature data correctly according to the following equations:

$$X_{pix} = \frac{X_i - \left(X_c - \frac{120 \times |Z_i|}{2 \times f_{ref}} \right)}{\text{PixelUnit} \times \frac{|Z_i|}{f_{ref}}}, Y_{pix} = \frac{Y_i - \left(Y_c - \frac{120 \times |Z_i|}{2 \times f_{ref}} \right)}{\text{PixelUnit} \times \frac{|Z_i|}{f_{ref}}}$$

Where, X_c, Y_c and Z_c are the coordinates of the point obtained when the laser is in its default position. X_{pix} and Y_{pix} are the coordinates of a pixel in the 2D IR image. They need to be rounded to an integer if X_{pix} or Y_{pix} is a float. Once the coordinates of the corresponding pixel is found, the temperature data was fused to the point in the 3D point cloud.

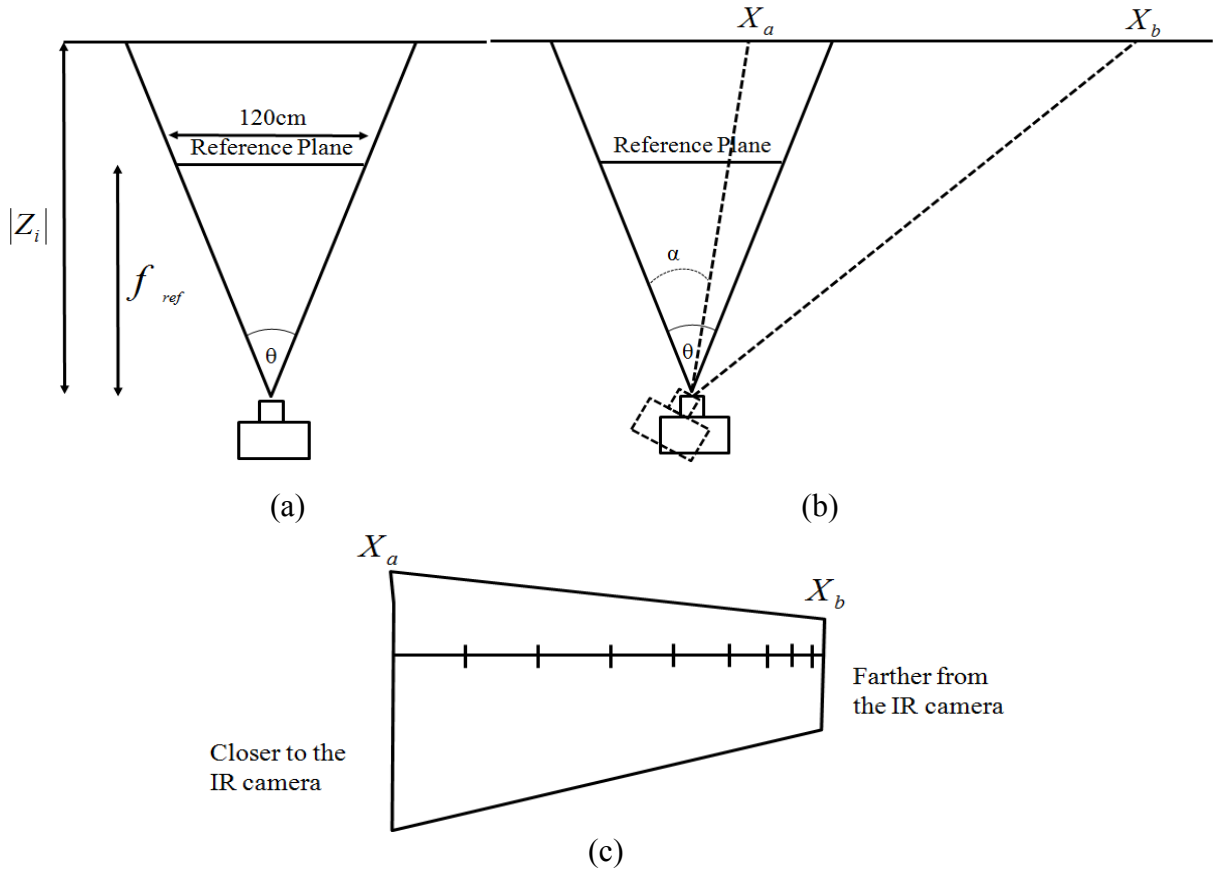


Figure 13. Illustration of data fusion process

As shown in Figure 13(b), the camera was rotated to obtain temperature data of another part of the point cloud. Under this circumstance, the reference plane is no longer parallel to the object.

Due to the effect of the perspective projection, objects in the distance appear smaller than objects close by. As shown in Figure 13(c), if we use simple interpolation and take equally spaced steps to compute pixel coordinates, a distorted image map will be resulted. To avoid such problem, the perspective correctness method is used in this research. The perspective correct mapping interpolates after dividing by depth Z_i , then uses its interpolated reciprocal to recover the correct coordinate (Hill and Kelley 2006):

$$X_\alpha = \frac{(1 - \alpha) \frac{X_a}{Z_a} + \alpha \frac{X_b}{Z_b}}{(1 - \alpha) \frac{1}{Z_a} + \alpha \frac{1}{Z_b}}, \text{ where } 0 \leq \alpha \leq 1$$

When the camera is rotated, the area of the camera view will vary based on the angle the camera is rotated by. The coordinates of the edge points in the IR image can be calculated using the following equations:

$$X_a = X_c + Z_c \tan\left(\alpha - \frac{\theta}{2}\right), X_b = X_c + Z_c \tan\left(\alpha + \frac{\theta}{2}\right)$$

Thus when the objects are not parallel to the camera, the temperature data can be mapped to 3D point clouds using following equations:

$$X_{pix} = \frac{X_i - X_a}{PixelUnit \times \frac{|Z_i|}{f_{ref}} \times \frac{1}{X_\alpha}}, Y_{pix} = \frac{Y_i - Y_a}{PixelUnit \times \frac{|Z_i|}{f_{ref}} \times \frac{1}{X_\alpha}}$$

3.1.2 Field Test

a) Test with part of a building

A part of the Peter Kiewit Institute building at University of Nebraska, as shown in Figure 14, was used to create a 3D thermal model. The test was conducted in a cloudy winter afternoon. The developed system was placed in front of the building parallel to the wall. 30 IR images were taken after 3D point clouds of the building were created. Through the data fusion process, all the available temperature data was mapped to the corresponding points. The point cloud was colored according to temperature value where dark blue represents no available temperature information, and red represents the higher temperature. As shown in Figure 15, some of areas of the wall are showing a higher temperature which means there is high possibility of heat loss. A simple mouse click on a point shows information about the surface of the building. For example, in Figure 15, the X, Y, and Z coordination of the selected point is (31.159, 118.633, -450.859), the intensity of this point is 159 which means the signal strength of the received laser light, and the temperature of this point is -8.719°C.



Figure 14. Digital image of the building

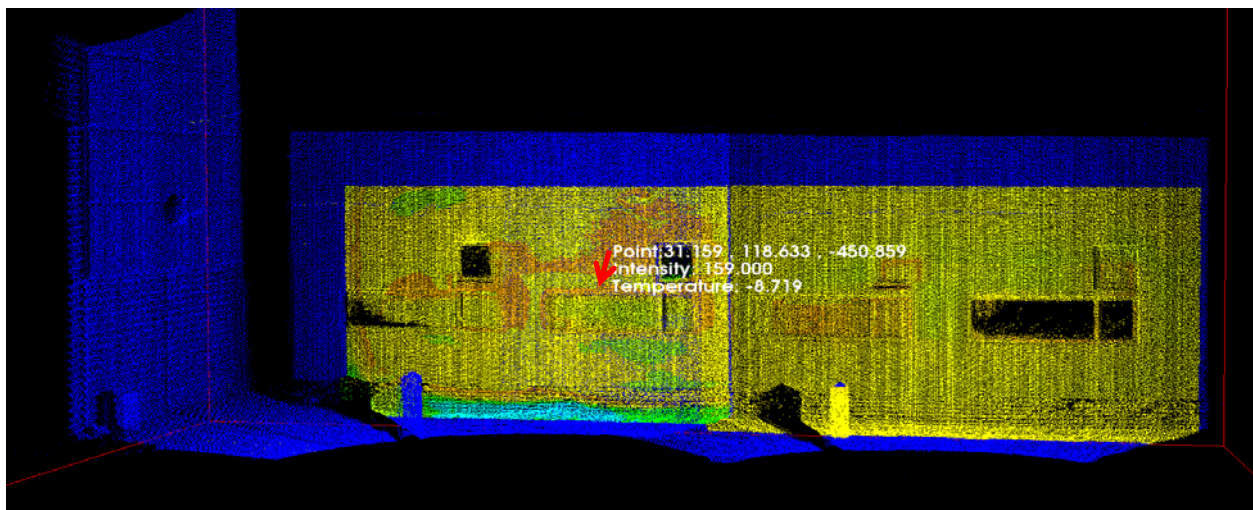


Figure 15. 3D energy performance model of the building

b) Test with a residential house

Another field test was conducted on a residential house which is shown in Figure 16. As shown in Figure 17, and 18, the 3D energy performance model of the house was created and rendered by different colors based on the different temperature values.



Figure 16. Digital image of the house

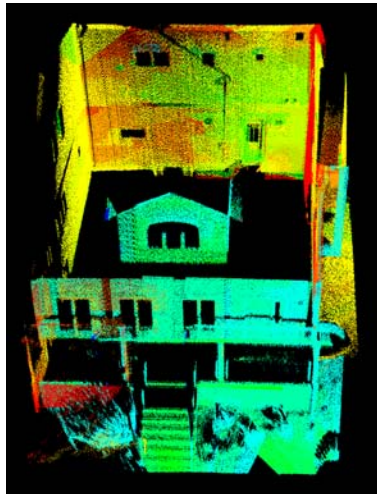


Figure 17. 3D energy performance model of the house (bird view)

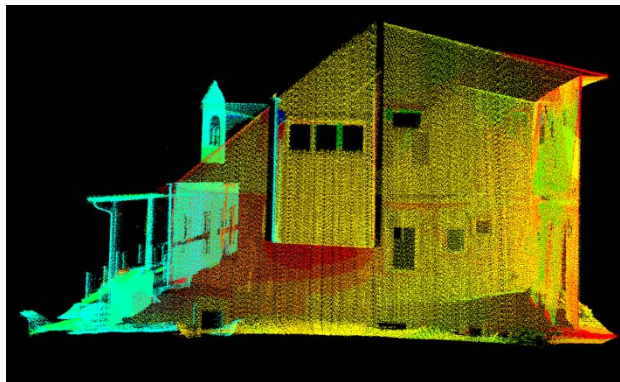


Figure 18. 3D energy performance model of the house (side view)

3.2 Development of Building Envelope Recognition Algorithm

3.2.1 Methodology

Building envelope is an important part of buildings when it comes to energy efficiency. It is a physical separator in which energy exchange with the environment can take place. The components of the building envelope include roof, walls, doors and windows. The dimensions and the positions of all these components are essential data in conducting energy analysis. Considering being transformed to gbXML file later, in this paper, the building envelope is divided into two categories according to gbXML schema: openings and surfaces.

The point cloud data tested in this chapter was obtained by using our developed 3D laser scanner as shown in Figure 19 which was customized by mounting a 2D line scanner on top of a pan-tilt-unit (PTU). During the scan, the 2D line scanner can capture different vertical planes while the PTU is being panned. All the points were stored in order by being scanned.

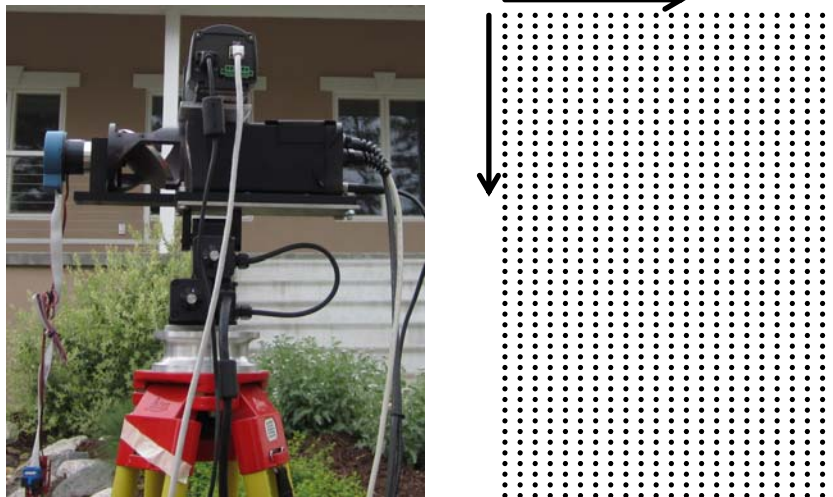


Figure 19. 3D laser scanner system (left) and the order of storing the obtained data

3.2.1.1 Openings

a) Windows

Usually there are few points reflected from the window glass, which will result in creating a large hole in the point cloud where there should be a window. Thus, the holes can be utilized to recognize the windows. As shown in Figure 20, for each point in the point cloud, it has to compare Y value with its next vertical neighbor point. If the absolute value of the difference between them is greater than 20 units, the point itself and its vertical neighbor point will be respectively marked as lower and upper window boundary points. In Figure 20, point P_a and

P_{a+l} are the first detected point pairs, and P_b and P_{b+l} are the last pair for the window area. Then these four points will be recognized as the corner points of this window, and the length and width of the window can be calculated by the formula (1),

$$Length = [(X_b - X_a) + (X_{b+l} - X_{a+l})] / 2, \quad Width = [(Y_a - Y_{a+l}) + (Y_b - Y_{b+l})] / 2 \quad (1)$$

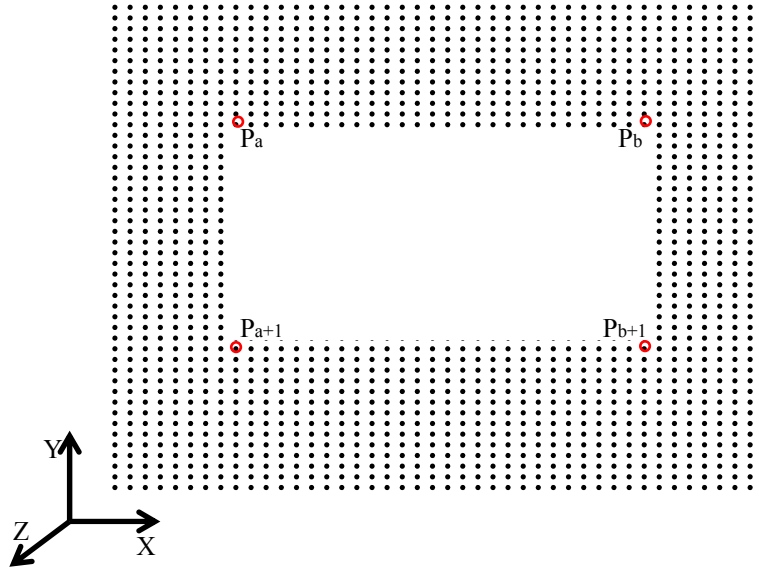


Figure 20. Schematic diagram of the window recognition

b) Doors

Usually doors are not on same plane with walls, as shown in Figure 21, from top view, it can be recognized that door and wall are on the different plane. In this paper, this means door plane has different Z value with wall plane. After conducting several tests, the empirical value of the Z value difference is set up as 3 to 5 units, which means that it will be recognized as a door if the difference of Z value is greater than 3 units and less than 5 units. Most of the time there is a small window in the door, and this can be also used as a condition to detect the door. In this paper, if the width of the detected window is smaller than 8 units. For example, in Figure 4, each point compares the Z value with its next vertical neighbor point. If,

$$3 < |Z_a - Z_{a-l}| < 5, \quad 3 < |Z_{a+n} - Z_{a+n+l}| < 5, \quad 3 < |Z_b - Z_{b-l}| < 5, \quad 3 < |Z_{b+n} - Z_{b+n+l}| < 5,$$

and also one small window in the door was recognized in advance by conducting the windows recognition algorithms, then points P_a , P_{a+n} , P_b , and P_{b+n} can be recognized as four corner points of the door, and the length and width of the door can be calculated by the formula (2),

$$Width = [(X_b - X_a) + (X_{b+n} - X_{a+n})] / 2, \quad Length = [(Y_a - Y_{a+n}) + (Y_b - Y_{b+n})] / 2 \quad (2)$$

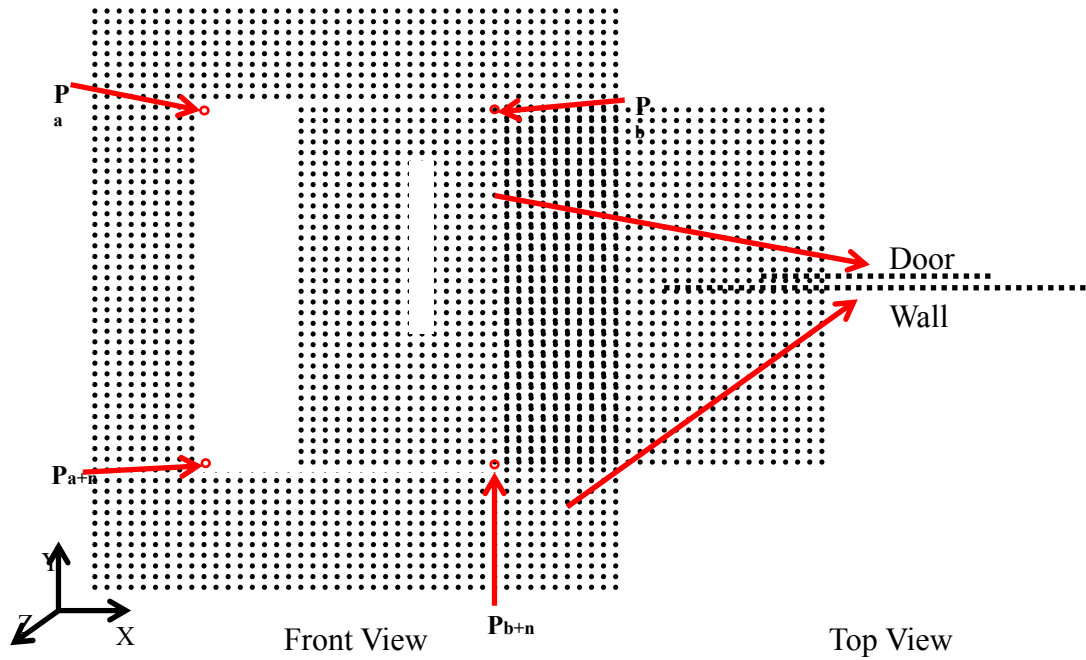


Figure 21. Schematic diagram of door recognition

3.2.1.2 Surfaces

a) Exterior Walls

As mentioned in the introduction section, simplistic geometric information is enough for BEP simulation tools. In this paper, the simplistic geometric outline of the building is detected as exterior walls. The developed algorithm for exterior walls recognition is using a similar concept with image gradient which is a directional change in the intensity or color in a 2D image. In the 3D point clouds, the points can be seen as pixels which have three attributes (X, Y, and Z). Building is usually composed of multiple planes, and the edge of any two different planes could create an outline of the building. In Figure 22, there are two different planes which have a common edge shown as a red line. The points in the left plane have the same Z value with 1 unit tolerance, and the points in the right plane have the same X value with 1 unit tolerance. This common edge line is recognized as part of the outline of the building. In the same way, other parts of the outline can be detected as well.

b) Roof

A roof was difficult to scan completely due to the overhang which blocked the laser beams and the tested house was located on the hill. In addition, our current 3D laser system has a short range measurement, so the roof was not included in the point clouds data. However, the outline of the roof were roughly recognized by our algorithm by connecting the top lines of the outlines

of the exterior walls because of its unique attribute that a roof always locates on top of the exterior walls.

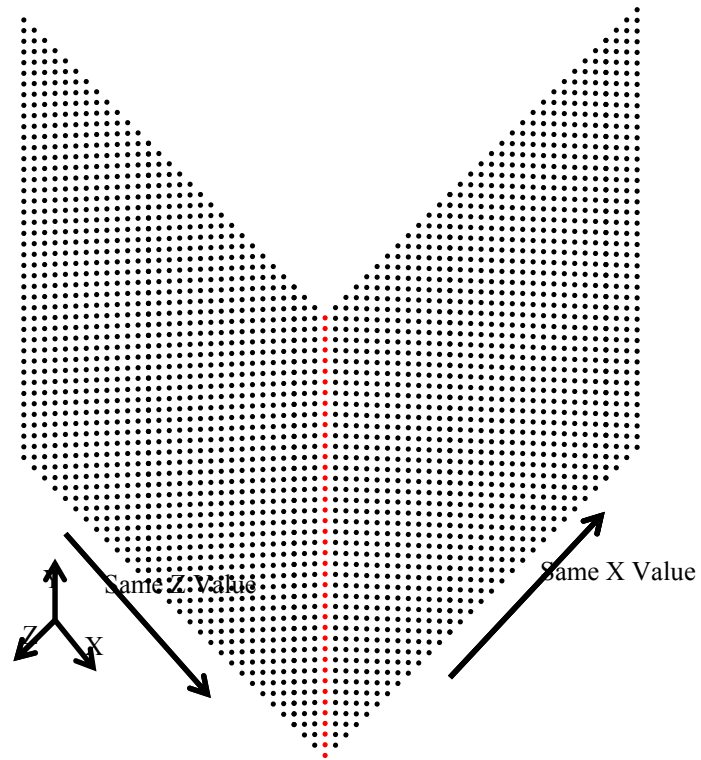


Figure 22. Schematic diagram of surface recognition



Figure 23. 3D point cloud and 2D digital image of a residential house

3.2.2 EXPERIMENTAL RESULTS

A preliminary test on a residential house was conducted, as shown in Figure 23, 3D point clouds data was successfully obtained and pre-processed. One side of the house was partially scanned because there is not enough space to set up our 3D laser system.

Figure 24 shows the testing results after being processed by using our building envelope recognition algorithm. In the results, different components were rendered in different colors. A simplistic geometric outline was successfully recognized, and both the front and back doors were also recognized. There are 34 windows in this residential house in total, and 21 of them were successfully recognized from the point cloud. Among the missing 13 windows, 9 of them were missing because the point cloud data didn't include them due to they are windows for basement thus blocked by the ground. The other four failed to be recognized because they are too small to be matched with the empirical value set up in the test. Figure 24 illustrates that each component of the building envelope can be recognized as an individual object which is an essential condition for BEP simulation and analysis. Precision and recall are used to measure the detection performance of the method (Olsen and Delon 2008). As shown in Table 2, TP stands for the number of correctly recognized components, FP means the number of wrongly recognized components, and FN is the number of components without being recognized. Then the detection precision and recall can be calculated according to the formula shown in Table 2.

Table 2. Precision and Recall of Doors and Windows Recognition for field test point cloud

| Component | TP | FP | FN | Precision (%) TP/(TP+FP) | Recall (%) TP/(TP+FN) |
|------------------|-----------|-----------|-----------|---|--|
| Doors | 2 | 0 | 0 | 100 | 100 |
| Windows | 21 | 0 | 4 | 100 | 84 |



Figure 24. 2D digital images and test results from top, left, back, and right view

3.3 Development of Web-Based 3d Building Performance Model

3.3.1 Methodology

The methodology proposed in this paper is mainly composed of the following steps, shown in Figure 25: (1) 3D point-cloud data with temperature ($^{\circ}\text{C}$) and thermal color information are obtained by a hybrid thermal laser scanner; (2) the 3D point-cloud data from the laser scanner in the Cartesian Coordinate System are converted into the data in the Geographic Coordinate System; (3) the converted point cloud data with temperature information are mapped on the prepared BIM model, then presented in Google Earth Pro™ in the form of KMZ 3D model, with different color base on the temperature degree.

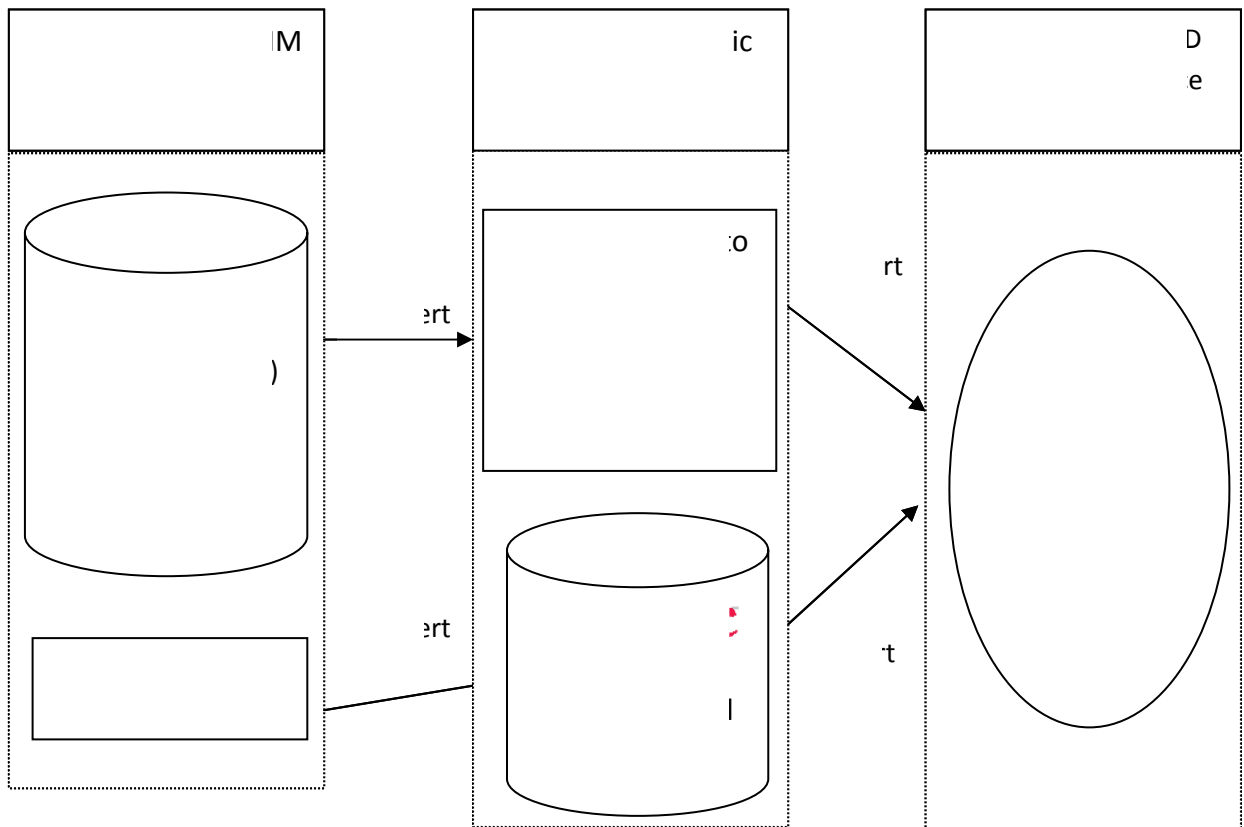


Figure 25.The process of the methodology

3.3.2 Creating Data

3D point cloud data with temperature ($^{\circ}\text{C}$) and thermal color information are obtained by a hybrid thermal laser scanner, which is composed of a laser scanner, Potable Test Unit (PTU) and a thermal camera, shown as Figure 26 (a)(Cho and Wang 2011; Wang et al. 2011; Wang and Cho 2011). A line laser is able to collect the data in a single vertical plane; while PTU rotates in a horizontal plane with a high resolution. Through combining both of these devices and resolving their kinematic problems, the 3D point-cloud data are generated; meanwhile, the thermal camera

works synchronously with the laser and PTU, and obtains the temperature ($^{\circ}\text{C}$) and thermal color information of the point cloud. Finally, 3D point cloud model with temperature ($^{\circ}\text{C}$) and thermal color information is obtained as shown in Figure 26(b).

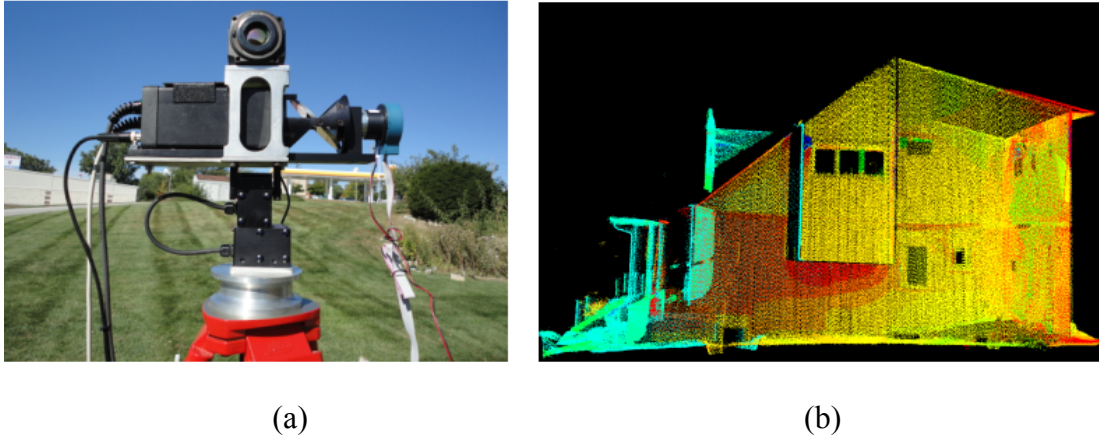


Figure 26. The hybrid thermal laser scanner (a) and 3D point clouds with thermal color codes (b)

3.3.3 Converting 3D Point Cloud Data to Geographic Coordinate Data

The point cloud's Cartesian coordinates (x, y, z) need to be converted to latitude, longitude, and altitude (LLA) coordinates to be imported to Google Earth Pro™ through using transformation between LLA and earth-centered, earth-fixed (ECEF) coordinates as shown in Figure 27.

Firstly, three LLA coordinates are measured by using GPS receiver; meanwhile, a minimum of three corresponding Cartesian coordinates of points with the same location in the point cloud are measured and stored. These LLA coordinates are then converted into ECEF coordinates through using the LLA2ECEF algorithm (Kleder 2005). Now three corresponding coordinates in two different coordinate systems are obtained, which are Cartesian coordinates and ECEF coordinates.

All the points in the point cloud can be converted to ECEF coordinates through applying the rotation matrix and translation matrix which can be obtained from processing the three corresponding pairs of coordinates. After being converted to ECEF coordinates, all the points can be converted to LLA coordinates through using ECEF2LLA algorithm (Kleder 2006). At last, all the Cartesian coordinates in the point cloud are converted to LLA coordinates.

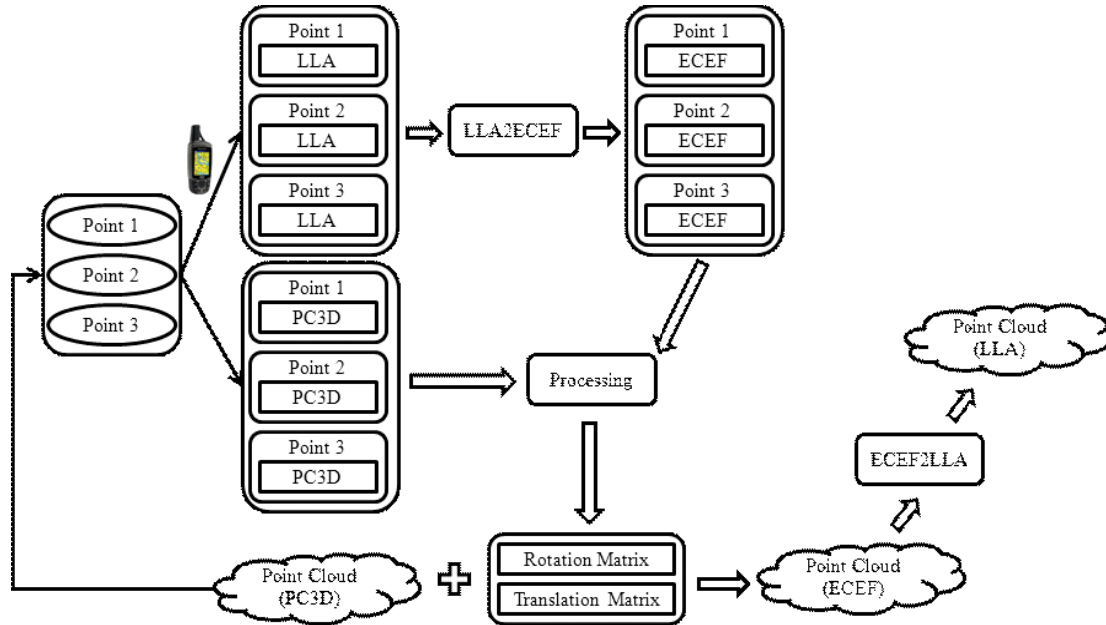


Figure 27. The process of converting Cartesian coordinates to LLA coordinates

3.3.4 Converting BIM model to KMZ, KML 3D Model

Building Information Modeling (BIM) involves representing a design as object, which is the process of generating and managing building data during its life cycle (Lee et al. 2006; Liu and Akinci 2009; Leite et al. 2009). It could be created by many different programs and uses three-dimensional, real-time, dynamic building modeling software to increase productivity in building design and construction (Yezioro et al. 2008; Eastman 2009). Therefore, the BIM models are compatible with many different file types such as KMZ which is acceptable file format for a BIM model to be imported to the Google Earth™. Thus, the KMZ format with geographic information such as location was selected as a main file format of the BIM model in this study. In addition, SketchUp™ (Google 2010) was used to build a KMZ based BIM model in the geographic coordinates converted from other common BIM formats modeled by a common BIM tools such as Revit™ and ArchiCAD™ (Figure 28, 29).

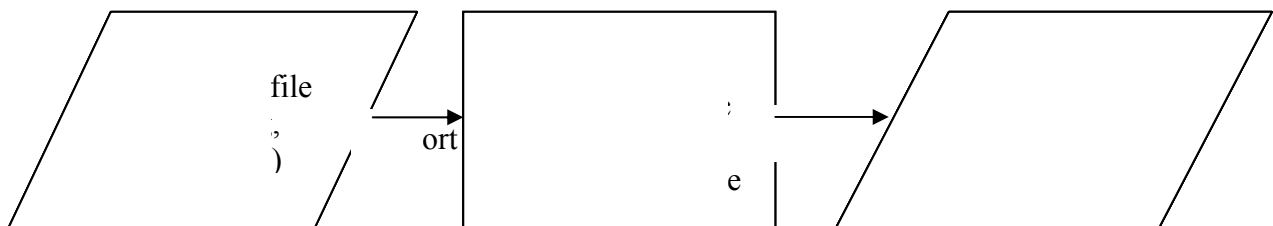


Figure 28. The process of converting BIM model to KMZ, KML 3D model

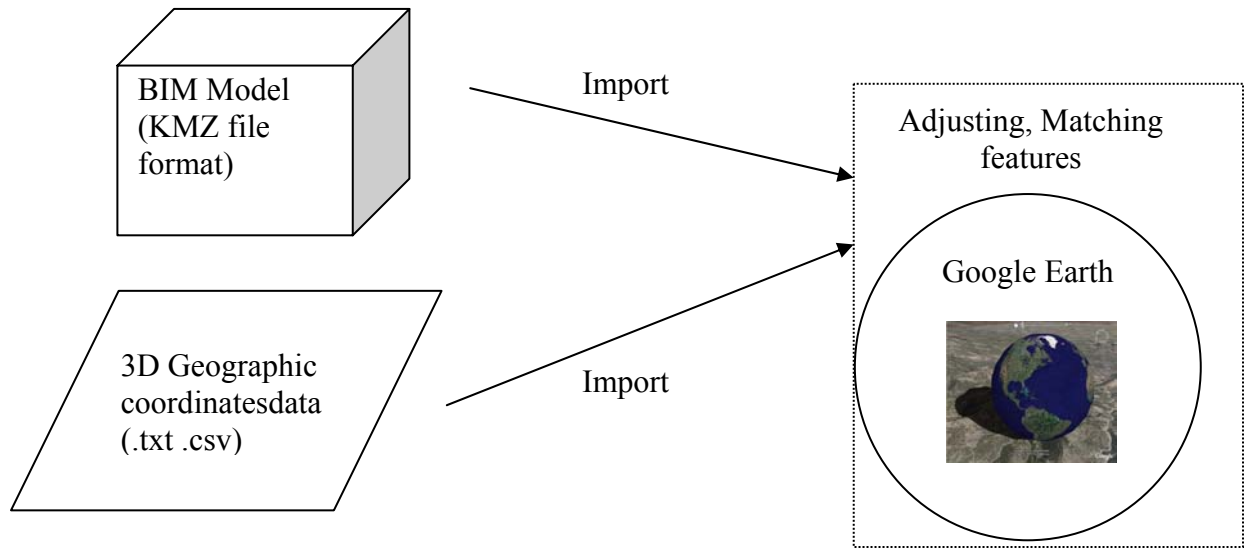


Figure 29. BIM and External data Integration Process in Google Earth Pro™

3.3.5 BIM with 3D Geographic Data in Google Earth Pro™

In the process of importing 3D geographic data into the Google Earth Pro™, it is important to determine errors or differences of the whole process in order to minimize the segmentation errors. The 3D point clouds include millions of points, which are imported as separate objects containing specific information such as temperature and GIS information. Therefore it is ineluctable that this set of data can be imported into the Google Earth Pro™ with some difficulties due to its data size. Considering this problem, 80% of the original points are downsized and then imported into the Google Earth Pro™. Furthermore, when the 3D point clouds, shown in Figure 30, are integrated with the existing BIM model as shown in Figure 31, another difficulty was to develop an accurate transforming matrix to transfer the locally scanned spatial data (x,y,z) into the geospatial coordinates (longitude, latitude, altitude) of actual building location and orientation in Google Earth Pro™. It is also challenging to adjust and match the BIM model to the 3D as-built geographic data in Google Earth Pro™. It is because as-planned BIM design was somewhat different from the as-built design. Figure 32 (a) and (b) show the results in Google Earth Pro™. Also, when any point is clicked in Google Earth Pro™, the latitude, longitude, height and temperature information of the place are shown accordingly. It should be noted that actual scale of the BIM model needs to be scaled down or the point clouds need to be scaled up to show point clouds on the building surface.

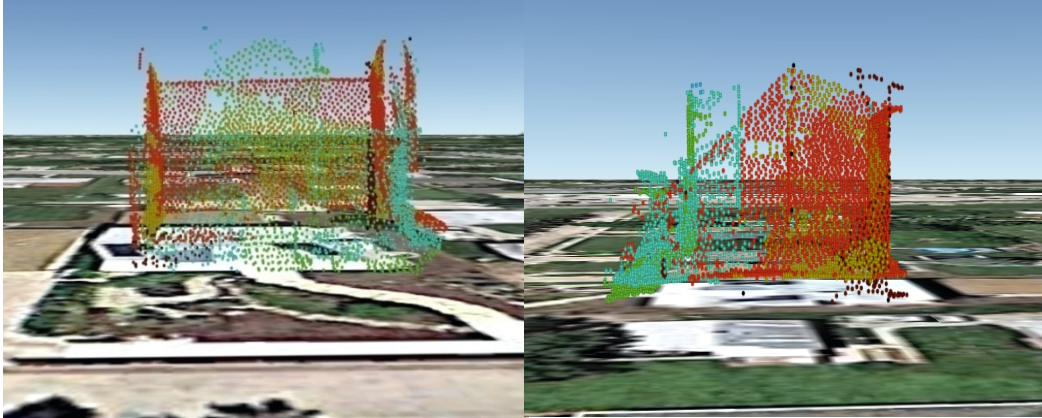


Figure 30. 3D Point Clouds in the Google Earth Pro™

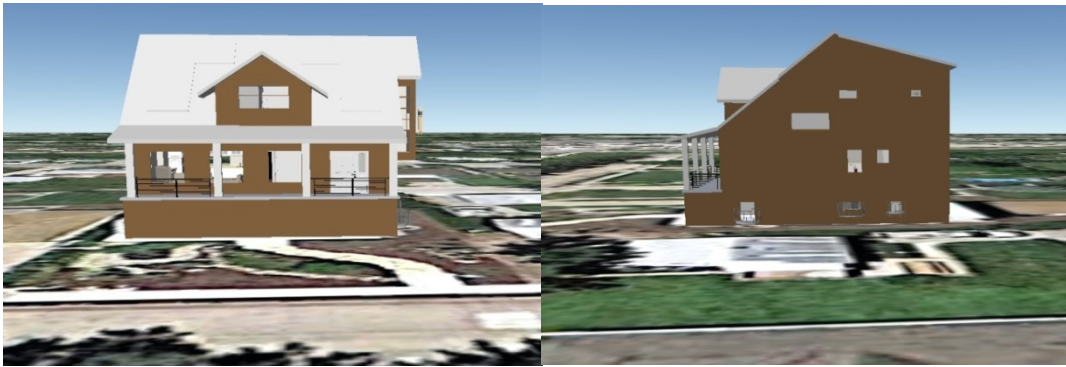
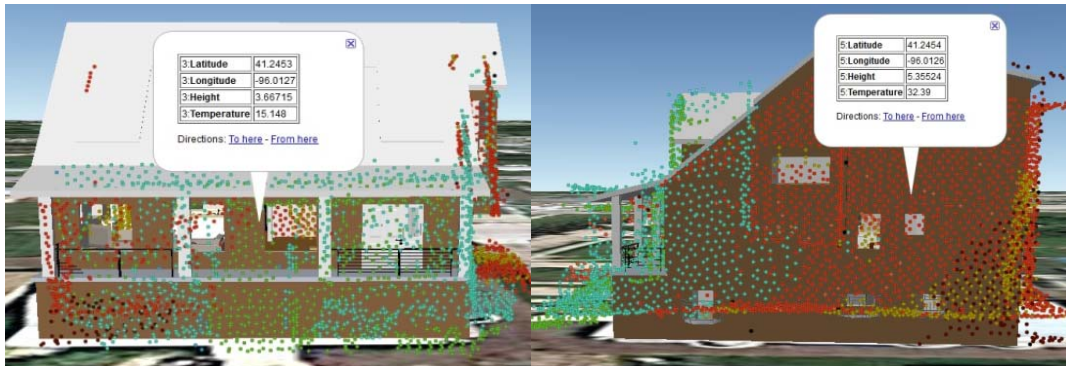


Figure 31. Imported BIM Model in the Google Earth Pro™



(a)

(b)

Figure 32. BIM Model with 3D point Cloud in Google Earth Pro™ with Temperature information

3.3.6 Thermal Information Marked by Different Colors

After the BIM model is integrated with 3D point clouds, it will be better if the 3D point clouds show different colors according to the different temperature range, which can help people quickly examine the building materials in order to make retrofit decisions based on the energy efficiency model. For this reason, the 3D points have been divided according to the different temperature range and imported different point colors with standard RGB values. Figure 33 and 34 show the results before and after the colors of the 3D point cloud are changed, respectively.

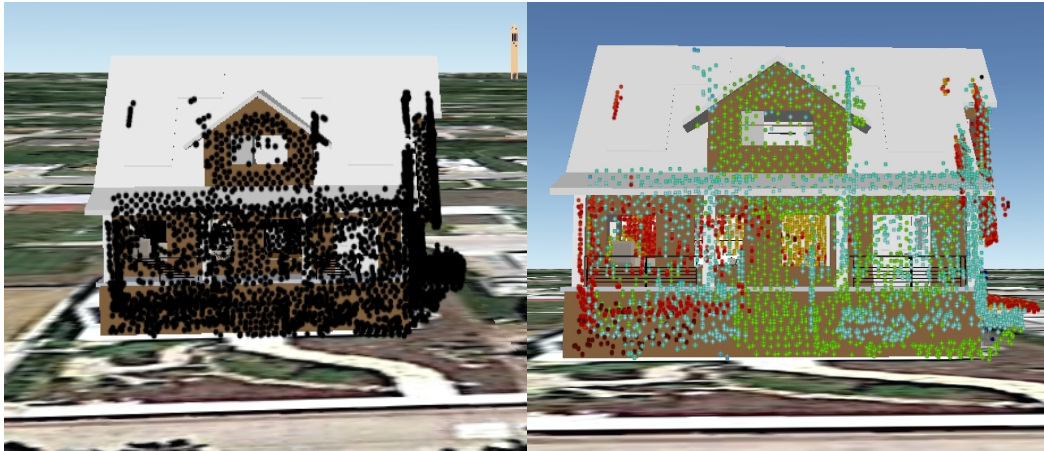


Figure 33. Before the colors are changed Figure 34. After the colors are changed

3.4 Hardware Development of a New 3D LiDAR System

In the previous sections, the data was collected by a short range laser scanner. To improve the quantity of the point cloud data, a new 3D LiDAR system was developed with two long-range laser scanners (80m). As shown in Figure 35, the system has been successfully built and currently under testing its functions. This new 3D LiDAR system will be taken outside to collect new point cloud data of the buildings.

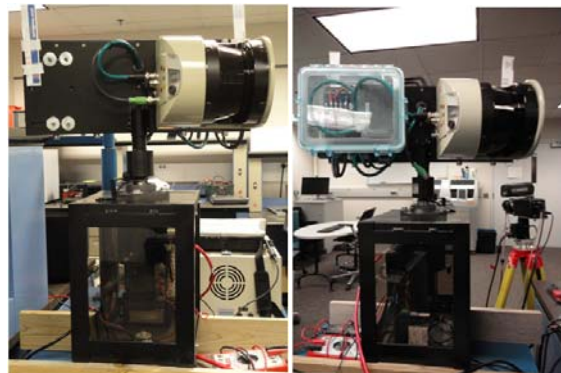


Figure 35. A developed new 3D laser system

4. Development of Automated Performance Diagnostics and Optimal Controls

4.1 Building field data collection and analysis

Theoretically, the building performance parameters are independent of the different heating periods; all the parameters should keep consistent throughout all the heating season.

From the results in Figure 36, it shows that the performance parameters' value are mostly stabilized with slight fluctuation, which was caused by the measurement accuracy and real building's unsteady internal thermal load.

However, from the statistical point of view, several t-tests were carried out, the results of which shows there is no statistically difference of these data.

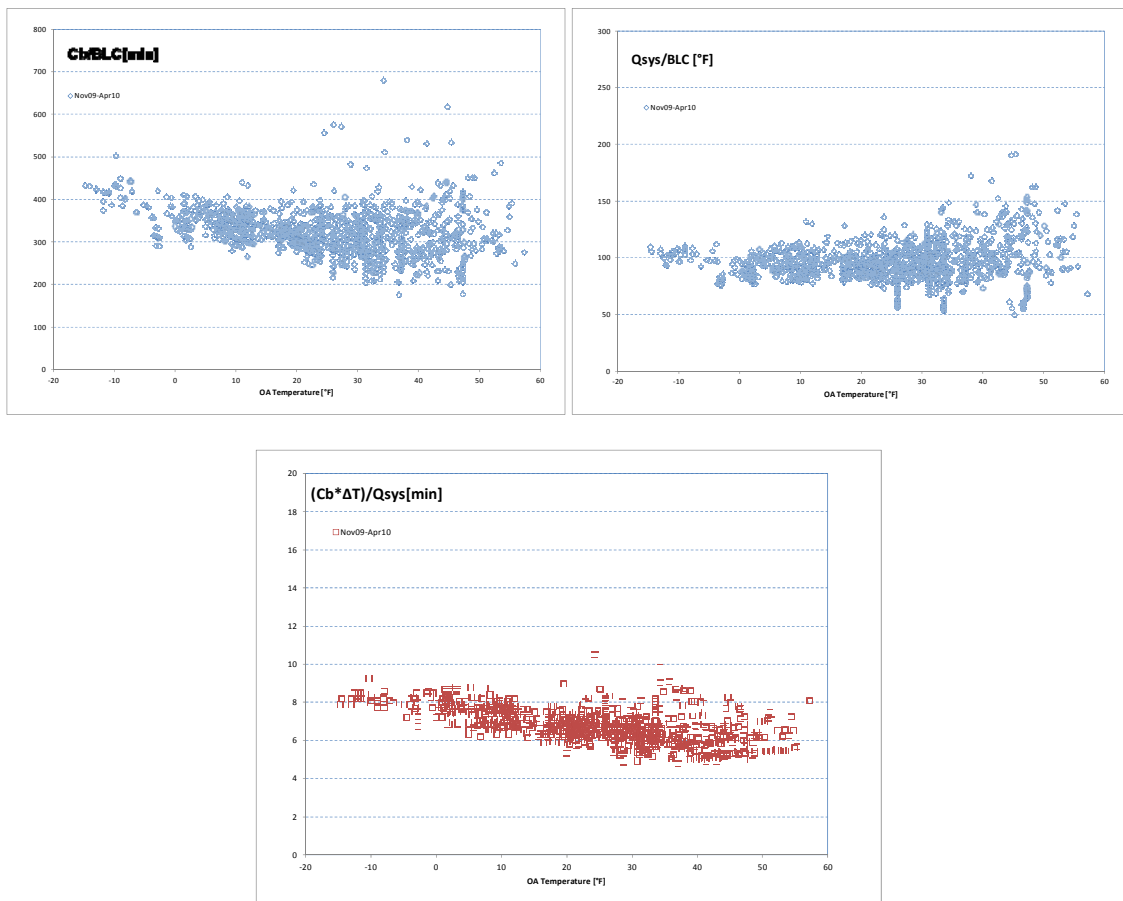


Figure 36. Field-test building performance data during heating season

4.2 Building American (BA) Benchmark

Building American is an industry-driven research program sponsored by the U.S. DOE that applies systems engineering approaches to accelerate the development and adoption of advanced building energy technologies in new and existing residential buildings.

The BA benchmark is generally consistent with mid-1990s standard practice, as reflected in the Home Energy Rating System (HERS) Technical Guidelines. Unlike other energy codes or reference homes used for HERS, ENERGY STAR, the benchmark represents typical construction at a fixed point in time.

The benchmark is intended for use with detached and attached single-family housing, as well as multi-family housing.

4.3 Standard Building Performance based on the BA Benchmark

The same house in the field test is selected to implement the benchmark definition in Omaha, NE. The benchmark simulation is implemented through energy plus for the building thermal load calculation under the local TMY2 weather file.

For the convenience of comparison, December is selected as the time period to implement the building thermal performance diagnosis.

Figure 37 shows the building benchmark performance parameters data, and these data are all preprocessed through infiltration of the day-time data with unstable internal thermal load. All these performance parameters also show a good stabilization, the statistical results of which is in Table 3.

Table 3 Field Test Results

| December | | Cb/BLC | $(Cb*\Delta T)/Q_{sys}$ | Q_{sys}/BLC |
|------------|-------|--------|-------------------------|---------------|
| | | [min] | [min] | [C] |
| Field Test | Avg | 330.88 | 6.76 | 98.5 |
| | Stdev | 36.27 | 0.61 | 12.69 |
| Benchmark | Avg | 120.07 | 4.89 | 49.17 |
| | Stdev | 18.01 | 0.20 | 7.39 |

4.4 Building Thermal Performance Diagnosis Methods

In the previous parts, a new methodology based on HVAC system cycle on/off time interval was developed to evaluate the building thermal performance, and the performance parameters are actually the unique features for this building which contains enough information of the building

envelope and mechanical system performance. The following step is to utilize these features to determine whether this building has good performance.

Two approaches are developed to provide the standard benchmark for the tested building performance parameters FDD.

- Direct Comparison with original building performance data

This approach is more direct and convenient when the object building is a new building constructed according to the benchmark standard, or an existing building which has already been evaluated through other ways such as field building energy audition, and so on.

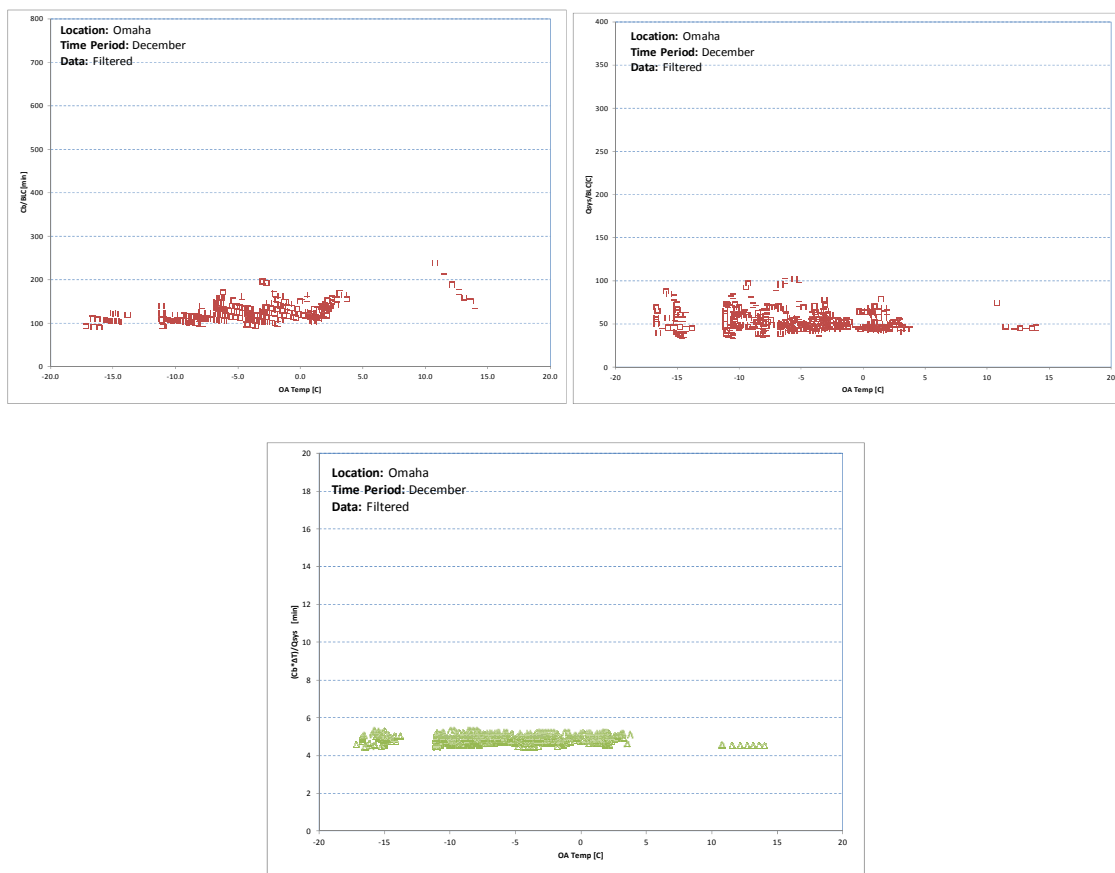


Figure 37. Benchmark Performance Data in December

For these object building, the thermal performance parameters data are recorded as the reference standard performance values, which will be compared with the future collected performance parameters.

The first approach is suitable for an existing building with a known good thermal performance to provide a standard for the reference to future maintenance and faults detection.

- Comparison with the Benchmark performance data

Through the simulated building with standard envelope and mechanical system performance, this method also is illustrated in the Figure 38.

Due to the limitation of the test buildings, only the second FDD method will be implemented to validate the building thermal performance parameters.

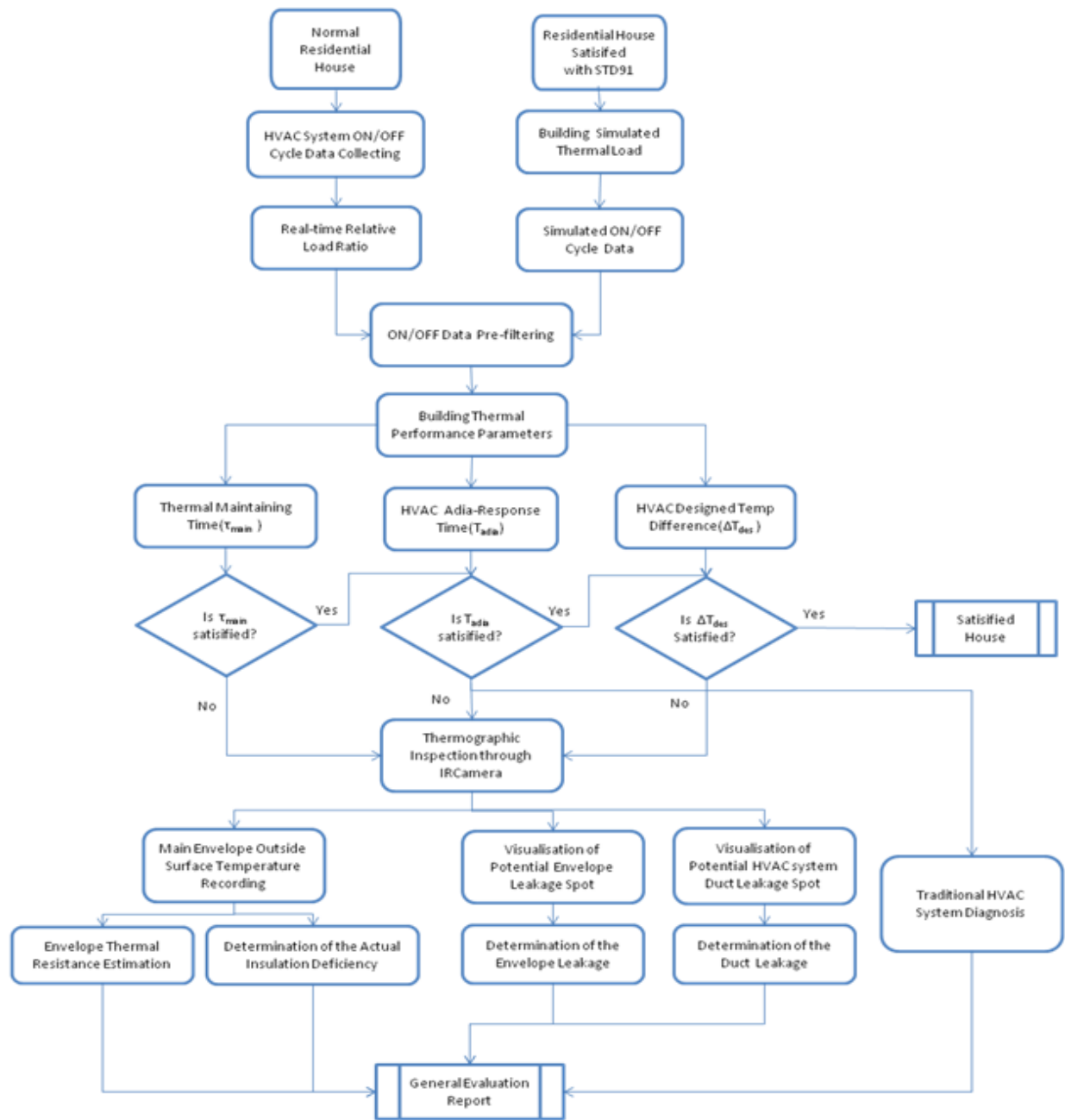


Figure 38. Flowchart of the thermal performance diagnosis based on benchmark

4.5 Building Thermal Performance Diagnosis based on the Benchmark

For the envelope parameter C_b/BLC , obviously the field value is larger than the simulation value, it means that the field building has a better whole building thermal performance than the standard benchmark, which could have better insulation for envelope, or be a tight building with less leakage.

For the mechanical system parameter $(C_b \cdot \Delta T)/Q_{sys}$, the field test value is larger than the simulation value, i.e., the field system heating capacity could be little smaller than the standard system heating capacity in the simulated benchmark situation.

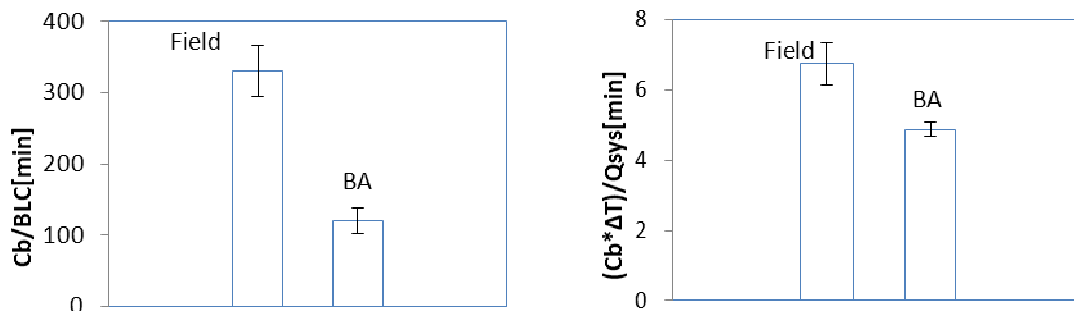
For the combined envelope and mechanical system performance parameter Q_{sys}/BLC , which is also a reflection of the heating design temperature difference, the field value is larger than the standard benchmark value.

Based on the above two parameters result, C_b/BLC and $(C_b \cdot \Delta T)/Q_{sys}$, the difference could be explained in that BLC contribute more than the Q_{sys} to the final value of the parameter Q_{sys}/BLC , which results in the larger field value.

In conclusion, the tested building has a better whole building thermal performance, while the mechanical system capacity probably degraded in comparison to the new design capacity. The final conclusion prove the method function well in evaluate the building thermal performance.

Actually, the tested building was building before 1970 when the envelope thermal insulation is not required, but this building shows a good thermal performance instead.

In the following part, the possible reasons are analyzed including the thermal mass effects and the infiltration impacts due to the mass wall and the tight construction compared to the current popular wood framed structure described in the benchmark standard.



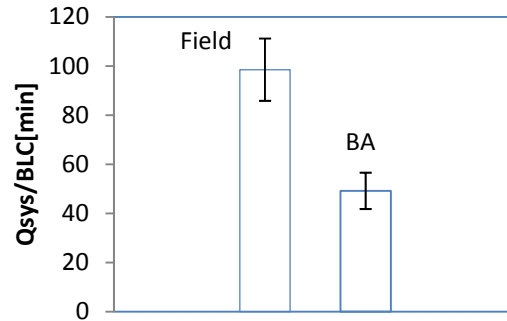


Figure 39. Performance Comparison between Benchmark (BA) and Field Test

4.6 Thermal mass effects

The ability to store energy and dampen the effect of temperature change on heating and cooling systems is known as the Thermal Mass Effect. Due to the mass effect, the performance R-value of the system can be two to three times greater than that of the material R-value, resulting in energy cost savings up to or exceeding 50%.

Since all U.S. thermal building standards including ASHRAE 90.1 and 90.2 and the American Building Benchmark are linked primarily to the steady-state clear wall R-value, calculating heating and cooling needs of a house built with high-mass walls is not straightforward. The steady-state R-value traditionally used to measure energy performance does not accurately reflect the dynamic thermal behavior of massive building envelope systems. This makes it difficult to evaluate the improved energy performance of massive building envelope systems.

- Comparative Analysis through Time Constant

The building walls can be modeled through 2R1C networks the equivalent 2R-C electric circuit i.e. including two resistances and one capacity.

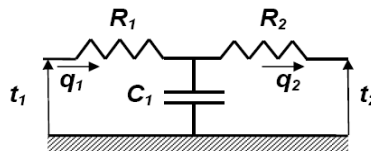


Figure 40. 2R1C network

The values of R_t and C_t for both high and low thermal mass walls are calculated and shown in Table 4 and 5.

Table 4 Benchmark Exterior Wall

| Code # | Description | Thickness [m] | Mass [kg/m ²] | Specific Heat [kJ/(kg.K)] | Resistance [(m ² .K)/W] | Capacitance [J/(m ² .K)] |
|--------|--------------------------------|---------------|---------------------------|---------------------------|------------------------------------|--------------------------------------|
| A0 | 0mm Outside Surface resistance | 0 | 0 | 0 | 0.059 | 0 |
| 609 | Lapped wood siding | 0.01 | 2.883 | 1.172 | 0.1 | 3378.876 |
| 608 | Plywood sheathing | 0.03 | 16.338 | 1.214 | 0.231 | 19834.332 |
| 116 | Insulation | 0.14 | 10.203 | 1.083 | 2.333 | 11049.849 |
| 620 | Gypsum wallboard | 0.01 | 8.009 | 1.088 | 0.059 | 8713.792 |
| E0 | 0mm inside Surface Resistance | 0 | 0 | 0 | 0.121 | 0 |
| ---- | Total | | ---- | ---- | 2.903 | 42993 |
| | | | | | RC[min] | 1951 |

Table 5 High Thermal Mass Wall with Standard Resistance

| Code # | Description | Thickness [m] | Mass [kg/m ²] | Specific Heat [kJ/(kg.K)] | Resistance [(m ² .K)/W] | Capacitance [J/(m ² .K)] |
|--------|--------------------------------|---------------|---------------------------|---------------------------|------------------------------------|--------------------------------------|
| A0 | 0mm Outside Surface resistance | 0 | 0 | 0 | 0.059 | 0 |
| A2 | 150*300mm Outer Brick | 0.30 | 203.5 | 0.79 | 1.332 | 160765 |
| 620 | Gypsum wallboard | 0.01 | 8.01 | 1.09 | 0.059 | 8730.9 |
| E0 | 0mm inside Surface Resistance | 0 | 0 | 0 | 0.121 | 0 |
| ---- | Total | | ---- | ---- | 2.903 | 471051 |
| | | | | | RC[min] | 21354 |

Obviously, the second exterior wall configuration has larger time constant value than the benchmark standard exterior wall. Theoretically, the ability to store energy and dampen the effect of temperature change on heating and cooling system is also in accordance with the time constant value sequence. Therefore, the second exterior wall has more mass effect, and also has better thermal performance envelope, and could result in less energy consumption of the thermal system.

- Comparative analysis through simulation

Simulation results analysis of the energy performance of light-weight and massive wall systems was presented in this part. Dynamic thermal performance of wall assemblies was investigated for

residential buildings and the potential energy savings were presented. It was found that some massive building envelope technologies can help in the reduction of building annual energies.

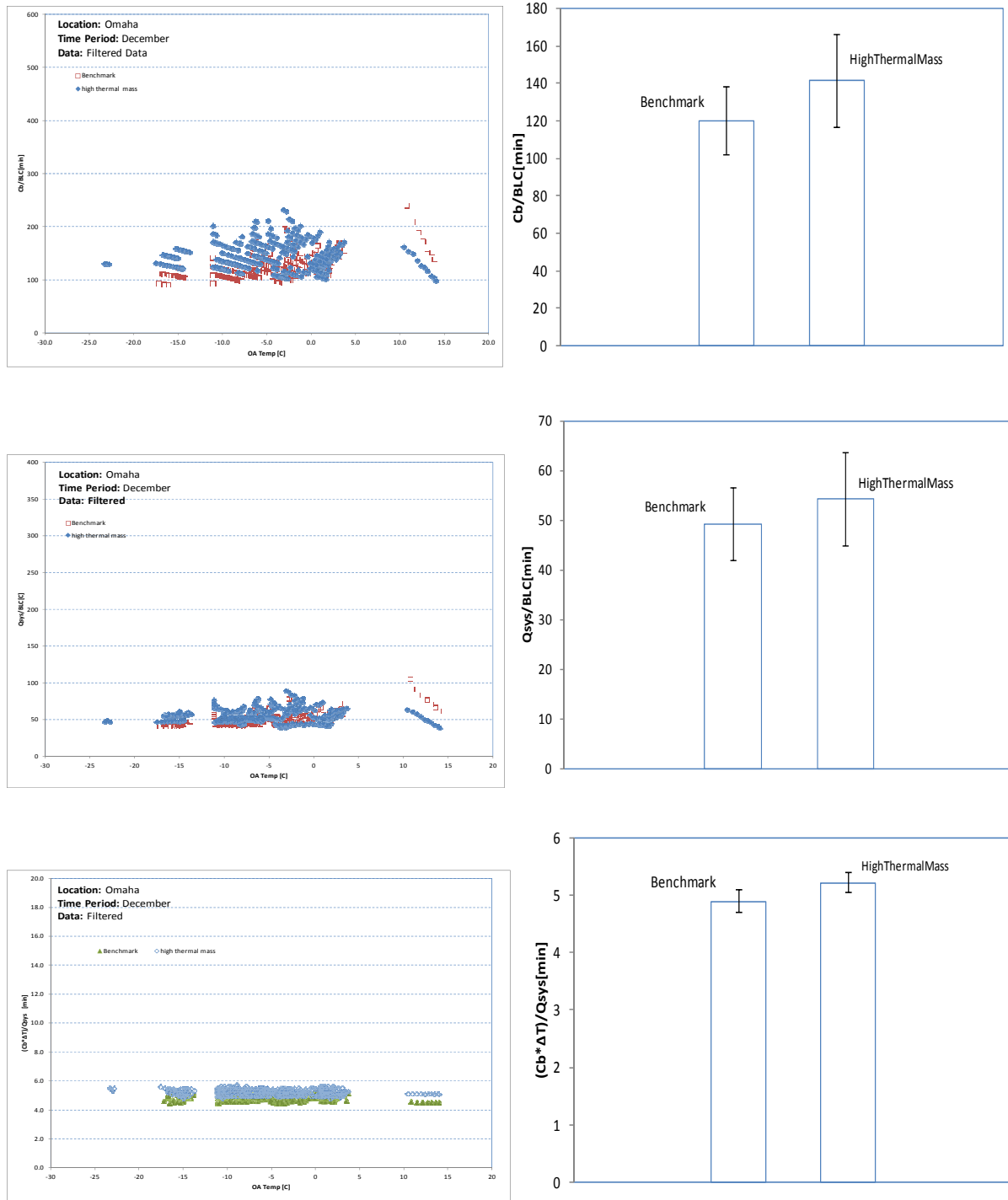


Figure 41. Comparison between Benchmark and High Mass Exterior Wall

As seen from Figures 41, the high thermal mass wall obviously has larger statistically value of C_b/BLC than the benchmark wall, which means the former thermal mass wall has smaller BLC, then exhibits a better whole building thermal insulation performance.

4.7 Infiltration effects

Three infiltration scenarios are implemented to show the infiltration impacts on the building thermal performance. As expected, the less the infiltration, the better the building thermal performance results of the three performance parameters.



Figure 42. Performance comparison among different infiltration scenarios

4.8 Blower Test for the whole building leakage

Professional energy auditors use blower door tests to help determine a home's air tightness.

These are some reasons for establishing the proper building tightness:

- Reducing energy consumption due to air leakage.
- Avoiding moisture condensation problems.
- Avoiding uncomfortable drafts caused by cold air leaking in from the outdoors
- Making sure that the home's air quality is not too contaminated by indoor air pollution.

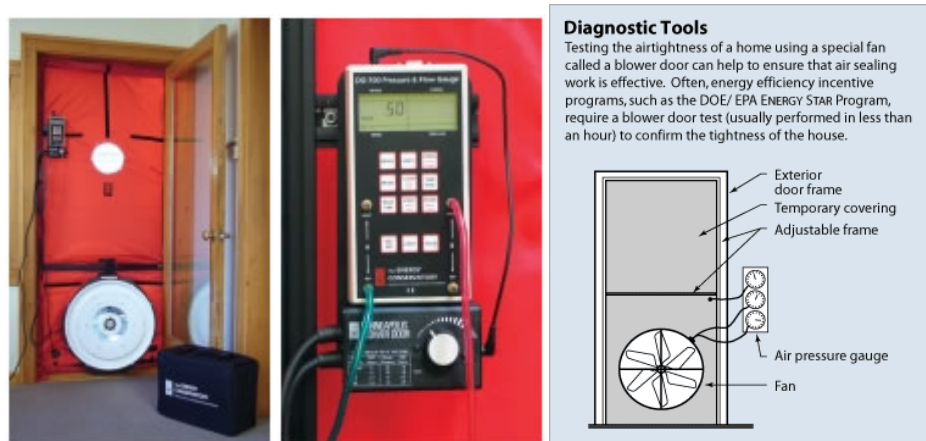


Figure 43. Blower Test

A blower door is a powerful fan that mounts into the frame of an exterior door. The fan pulls air out of the house, lowering the air pressure inside (Figure 43). The higher outside air pressure then flows in through all unsealed cracks and openings. The auditors may use a smoke pencil to detect air leaks. These tests determine the air infiltration rate of a building.

Blower doors consist of a frame and flexible panel that fit in a doorway, a variable-speed fan, a pressure gauge to measure the pressure differences inside and outside the home, and an airflow manometer and hoses for measuring airflow.

There are two types of blower doors: calibrated and uncalibrated. It is important that auditors use a calibrated door. This type of blower door has several gauges that measure the amount of air pulled out of the house by the fan. Uncalibrated blower doors can only locate leaks in homes. They provide no method for determining the overall tightness of a building. The calibrated blower door's data allow the auditor to quantify the amount of air leakage and the effectiveness of any air-sealing job.

4.8.1 Preparing for a Blower Door Test

Take the following steps to prepare your home for a blower door test:

- Close windows and open interior doors

- Turn down the thermostats on heaters and water heaters
- Cover ashes in wood stoves and fireplaces with damp newspapers
- Shut fireplace dampers, fireplace doors, and wood stove air intakes.

4.8.2 Blower Door Installation

1. Install Panel in Door Opening
 - a. Frame retainer clip
 - b. Adjust frame to loose fit in door
 - c. Install nylon cover
 - d. Reinstall frame to a tight fit
2. Install Fan in Door Panel
3. Install Gauge Module and pressure hoses
4. Electrical connections

4.8.3 Test Procedure

1. Set fan switches (low speed to start) and turn on fan
2. Adjust fan speed to achieve 50 Pa of pressure (House gauge)
3. Read Air Flow at selected pressure (High or Low Flow gauge)
4. If unable to reach 50 Pa,

Air Flow = flow read at Pressure (y) X Factor (z) (See Figure 44)

| Pressure (y) | Factor (z) |
|-----------------|---------------|
| 50.0 | 1.00 |
| 43.6 | 1.09 |
| 37.4 | 1.20 |
| 31.1 | 1.36 |
| 24.9 | 1.57 |
| 18.7 | 1.89 |
| 12.5 | 2.46 |
| 6.2 | 3.86 |

Figure 44. Pressure and corresponding factor

4.8.4 Flow Rate Reading

Airflow (cfm) = _____ at _____ Pa

Calculate air changes per hour (ACH)

ACH = 60 * Airflow(cfm) * Factor / 17 * HouseVolume = 60 * _____ * _____ / 17 * _____

Online Video Demo on Blower Door Test:

<http://www.youtube.com/watch?v=d0wE1kygj3Q>

Two different thermal insulation of exterior wall

The simulation results while envelope exterior wall lack of thermal insulation

- **Exterior Wall Structure 1**

Table 6 Exterior Wall Thermal Resistance

| Code # | Description | Thickness [in] | Density [lbm/ft ³] | Specific Heat [Btu/(lb.R)] | Resistance [(ft ² .F.h)/Btu] |
|--------|-------------------------|----------------|--------------------------------|----------------------------|---|
| 603 | Common structural brick | 3.5 | 150.0 | 0.1900 | 0.45 |
| 608 | Plywood | 0.75 | 34.0 | 0.2900 | 1.2 |
| 801 | Vertical Air space | 0.75 | 0.075 | 0.2400 | 0.9 |
| 100 | 2×4 wood frame wall | 3.5 | 7.06 | 0.2775 | 1.12 |
| 620 | Gypsum wallboard | 0.75 | 50.0 | 0.2600 | 0.75 |
| ---- | Total | 9.25 | ---- | ---- | 4.42 |

The simulation results while envelope exterior wall includes standard thermal insulation

- **Exterior Wall Structure 2**

Table 7 Brick Exterior Wall Thermal Resistance

| Code # | Description | Thickness [ft] | Density [lbm/ft ³] | Specific Heat [Btu/(lb.R)] | Resistance [(ft ² .F.h)/Btu] |
|--------|-------------------------|----------------|--------------------------------|----------------------------|---|
| 603 | Common structural brick | 0.67(8") | 150 | 0.19 | 0.9 |
| 1 | Wood furring/vertical | 0.06(0.75") | / | / | 0.9 |

| | | | | | |
|------|--------------------------------|-------------|-------|------|--------------|
| | air space | | | | |
| 727 | Expanded polystyrene sheathing | 0.17(2.75") | 2.65 | 0.29 | 13.75 |
| 620 | Gypsum wallboard | 0.06(0.75") | 50.00 | 0.26 | 0.5 |
| ---- | Total | | | ---- | 16.05 |

Table 8 Thermal performance parameters results for 3 different scenarios

| | | Cb/BL C | (Cb*ΔT)/Qs ys | Qsys/BL C | Qsys (Design) | BLC | Cb | Qsys (Cal) |
|---------------------|------------|---------|---------------|-----------|----------------|-------|------|------------|
| December | | [min] | [min] | [C] | [W] | [W/K] | kJ/K | [W] |
| Field Test | Avg | 330.88 | 6.76 | 98.5 | / | 64.1 | 1273 | 6318 |
| Brick Wall 1 | Avg | 77.08 | 2.8 | 55.2 | 16100 | 275.4 | 1273 | 15200 |
| Brick Wall 2 | Avg | 395.11 | 7.5 | 103.8 | 6150 | 53.7 | 1273 | 5576 |

4.8.5 Blower Door Test Result

4.8.5.1 Basic Input and Data Recording

Indoor Temperature (F)

Outdoor Temperature (F)

Location Climate Characteristics

Heating Degree Days (F)

Energy Climate Factor

Design Winter Temperature Differential

Design Winter Wind Speed (mph)

Cooling Degree Days (F)

Vent Weather Factor

Design Summer Temperature Differential

Design Summer Wind Speed (mph)

to Building Info

to Comments

[Help](#)

Test Mode

Pressurize

Depressurize

Method

Manual

Auto

Auto Test Parameters

Samples per Station:

Fan Adjust Rate:

Target Tolerance (Pa):

Building High Pressure Limit (Pa):

Fan Start (%):

[Restore Factory Settings](#)

Test Pressures

CGSB

CUSTOM

[Edit Custom Pressures](#)

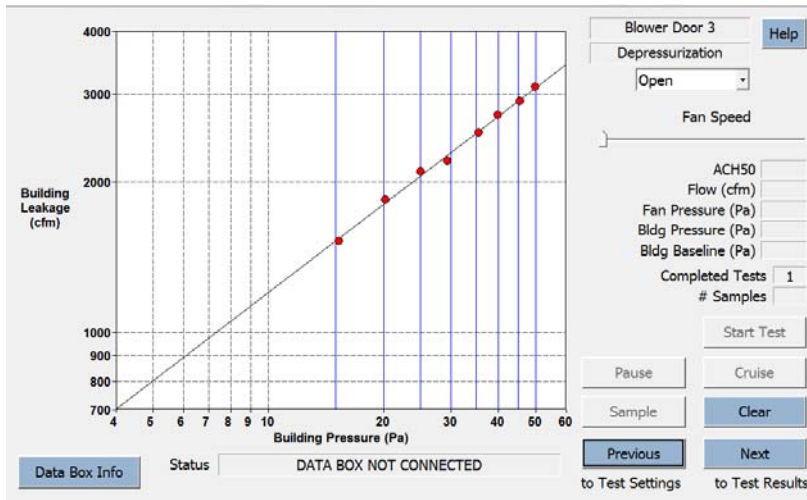
Zonal Pressures

Active

[Settings](#)

[Previous](#) [Next](#)

to Comments to Test Graph



[Help](#)

Airflow at 50 Pascals

3099 CFM (+/- 0.8 %)

6.20 ACH

0.86 CFM per ft2 floor area

0.56 CFM per ft2 surface area

Estimated Annual Infiltration

206.0 CFM 0.41 ACH

51.5 CFM per person

Leakage Areas

354.0 in2 (+/- 2.0 %) Canadian EqLA @ 10 Pa

199.4 in2 (+/- 3.5 %) LBL ELA @ 4 Pa

Estimated Design Infiltration

Winter: 344.4 CFM 0.69 ACH

Summer: 191.5 CFM 0.38 ACH

Building Leakage Curve

Flow Coefficient (C) = 311.8 (+/- 5.6 %)

Exponent (n) = 0.587 (+/- 0.016)

Correlation Coefficient = 0.99787

Mechanical Ventilation Guideline

Recommended Whole Building Mechanical Ventilation Rate: 0.0 CFM

Estimated Cost of Air Leakage

[Previous](#)

to Test Graph

Figure 45. Basic input and data recording

4.8.5.2 Result Analysis

- Benchmark reference source:

Building America Research Benchmark Definition (updated December 2009)

The hourly natural air change rate for a single-family home (detached or attached) benchmark shall be calculated based on the specific leakage area (SLA) determined using below Equation:

$$\mathbf{SLA = ELA / CFA = 0.00057}$$

Where:

ELA = effective leakage area (ft²), defined as the amount of open area that would result in the same total air exchange as the actual leakage area of the house at a pressure of 4 Pa.

CFA = conditioned floor area (ft²)

- Objective house

ELA: 199.4 in² (+/- 3.5%) LBL ELA @4Pa

CFA = 1196 + 1196 + 1069 = 3461 ft²

Then,

$$\mathbf{SLA = ELA/CFA = 0.00039}$$

5. CONCLUSION

In this project, a low-cost building information modeling method was introduced in which digital image processing techniques are utilized to extract house information from the images of houses. The developed floor plan frame recognition algorithm and vertical view information extraction algorithm are discussed. Through these two developed algorithms, the elevation view and vertical view information can both be obtained rapidly. About 90 house images were processed in our test with the developed algorithms with a 95% success rate. We show the feasibility to create “virtual” representations for the energy and environmental performance of existing buildings.

Secondly, a non-invasive 3D energy performance modeling method was introduced in this paper using the developed hybrid system which consists of a 3D LIDAR and an IR camera. In this method, a 3D as-built model of the building can be rapidly created by scanning the building using the hybrid system. Additionally, thermal image distortion was reduced by a uniquely developed IR camera calibration approach so that temperature information can be more accurately mapped to the 3D model. Furthermore, the information of each point in the building model can be accessed so that people can obtain the correct data for other applications such as heat loss calculation, thermal resistance calculation, and building energy simulation. In the preliminary field test, 3D energy performance models for a building and a residential house were created, and these models were easily used to obtain all relevant information including coordinates, intensity, and temperature of the points from the developed graphical user interface. An automated building envelope recognition algorithm was also introduced to recognize all the building envelope components from the 3D point cloud. Methodologies of recognizing windows, doors, exterior walls, and roof were all discussed in this paper. Through a field test on a residential house, the developed algorithm was tested and achieved very positive preliminary results in which different building envelope components were recognized as individual objects and rendered in different colors. There are still several challenges for this approach, such as difficulty of recognizing free shape components precisely, and extracting outlines of complicated types of residential roofs. Also, currently we are developing a long-range outdoor laser scanner to obtain better point clouds of buildings since the current version of our laser scanner was developed mainly for short-range indoor scanning purposes. In spite of these limitations, the proposed algorithm still states a feasible way to obtain all the essential information from the 3D as-is point cloud for the BEP analysis. To make the developed 3D energy performance model be easily accessible, another methodology was illustrated that how to make it accessible in web-based software, such as Google Earth. With all the testing results, it shows that the proposed methodologies have high potential to help the decision makers to improve their buildings by

providing reliable and visualized information of their building's energy performance through easily accessible web-based geospatial tools.

Finally, models have been developed and evaluated to predict and estimate operating performance for building systems, including HVAC equipment and building envelop. These models can be used to for automated performance diagnostics and optimal controls.

REFERENCES

- Bouguet, J.(2010). "Camera Calibration Toolbox for Matlab." <http://www.vision.caltech.edu/bouguetj/calib_doc/> (Jul. 9, 2010)
- Cho, Y. K., and Martinez, D. (2009). "Light-weight 3D LADAR System for Construction Robotic Operations. *Int.Symp.on Automation and Robotics in Construction*, IAARC, Austin, TX, 237-244.
- Cho, Y. K. and Wang, C. (2011). "3D Thermal Modeling for Existing Buildings Using Hybrid LIDAR System," *Proceedings of the 2011 ASCE International Workshop on Computing in Civil Engineering*, Miami, doi: 10.1061/ 41182(416)68
- Drennan, M. (2010). "An Implementation of Camera Calibration Algorithms." <http://www.ces.clemson.edu/~stb/ece847/projects/Camera_Calibration.pdf>
- Eastman, C. (2009). *Building Information Technology: Digital Building Lab @ Georgia Tech*. Retrieved April 9, 2011, <<http://bim.arch.gatech.edu/?id=402>>.
- Energy Information Agency(EIA), (2009). "Annual Energy Review 2008", DOE/EIA-0384 (2008), U.S. Department of Energy, June 2009.
- Golparvar-Fard, M., Pena-Mora, F., Arboleda, C. A., and Lee, S., "Visualization of Construction Progress Monitoring with 4D Simulation Model Overlaid on Time-Lapsed Photographs", *ASCE Journal of Computing in Civil Engineering*, Vol. 23(6), pp. 391-404, 2009.
- Google.(2010). "What makes SketchUp great". <<http://sketchup.google.com/intl/en.>>.
- Heikkila, J., and Silven, O. (1997). "A Four-step Camera Calibration Procedure with Implicit Image Correction." *IEEE Computer Society Conference on Computer Vision and Pattern Recognition*, IEEE, San Juan, Puerto Rico, 1106-1112.
- Hill, F. S., and Kelley, S. M. (2006). "Rendering Faces for Visual Realism." *Computer graphics: using OpenGL*, Pearson Prentice Hall, Upper Saddle River, NJ.
- Kleder, M. (2005). "Covert lat, lon, alt to ECEF Cartesian," <<http://www.mathworks.com/matlabcentral/fileexchange/7942-covert-lat-lon-alt-to-ecef-cartesian>>.
- Kleder, M. (2006). "Convert Cartesian (ECEF) Coordinates to lat, lon, alt," <<http://www.mathworks.com/matlabcentral/fileexchange/7941-convert-cartesian-ecef-coordinates-to-lat-lon-alt>>.

- Lee, G., Sacks, R., and Eastman, C. M. (2006). "Specifying parametric building object behavior (BOB) for a building information modeling system." *Automation in Construction*, 15(6), 758–776.
- Leite, F., Akinci, B., Garrett, J., and Akin, O. (2009). "Representation of Facility Contents and Threats for Supporting Identification of Vulnerabilities in Building Emergencies." In: *Proceedings of the 2009 ASCE Computing in Civil Engineering Conference*, Austin, TX.
- Liu, X. and Akinci, B. (2009). "Requirements and Evaluation of Standards for Integration of Sensor Data with Building Information Models." In: *Proceedings of the 2009 ASCE Computing in Civil Engineering Conference*, Austin, TX.
- Ma, L., Chen, Y., and Moore, K. L. (2003). "A New Analytical Radial Distortion Model for Camera Calibration." *IEEE Computer Society Conference on Computer Vision and Pattern Recognition*, IEEE, Madison, WI.
- Riaz, M., Kang, G., Kim, Y., Pan, S., and Park, J., "Efficient Image Retrieval Using Adaptive Segmentation of HSV Color Space", *International Conference on Computational Sciences and Its Applications ICCSA*, pp 491-496, 2008.
- U.S. Department of Energy (DOE) (2008). "2008 U.S. DOE buildings energy databook," <<http://buildingsdatabook.eren.doe.gov/>>
- Wang, C., Peng, Y., Cho, Y. and Li, H. (2011). "As-Built Residential Building Information Collection and Modeling Methods for Energy Analysis." *Proceedings of the 28th International Symposium on Automation and Robotics in Construction (ISARC)*, Seoul, Korea, June 29-July 2, pp.226-231
- Wang, C., Cho, Y. (2011). "Non-invasive 3D Thermal Modeling for Buildings," *ASCE, International Conference on Sustainable Design and Construction in Kansas City, MO*.
- Yezioro, A., Dong, B., and Leite, F. (2008). "An Applied Artificial Intelligence Approach towards Assessing Building Performance Simulation Tools." In: *Energy and Buildings*, Volume 40, Issue 4, p. 612-620